ORIGINAL ARTICLE

Rice increases phosphorus uptake in strongly sorbing soils by intra-root facilitation

Christian W. Kuppe[1, 2] | Guy J. D. Kirk[3] | Matthias Wissuwa[4] | Johannes A. Postma[1]

[1]Forschungszentrum Jülich GmbH, Institute of Bio- and Geosciences – Plant Sciences (IBG-2), 52425 Jülich, Germany

[2]RWTH Aachen University

[3]School of Water, Energy and Environment, Cranfield University, Cranfield MK43 0AL, UK

[4]Crop, Livestock and Environment Division, Japan International Research Center for Agricultural Sciences, Tsukuba, Japan

Correspondence
Christian Kuppe, Forschungszentrum Jülich GmbH, Institute of Bio- and Geosciences – Plant Sciences (IBG-2), 52425 Jülich, Germany
Email: c.kuppe@fz-juelich.de

Funding information
CK and JP were institutionally funded by the Helmholtz Association (POF IV: 2171, Biological and environmental resources for sustainable use). GK was supported by BBSRC (Grant Ref. BB/R020388/1) and OCP (Cranfield-Rothamsted-UM6P Collaboration Grant).

Upland rice (*Oryza sativa*) is adapted to strongly phosphorus (P) sorbing soils. The mechanisms underlying P acquisition, however, are not well understood, and models typically underestimate uptake. This complicates root ideotype development and trait-based selection for further improvement. We present a novel model, which correctly simulates the P uptake by a P-efficient rice genotype measured over 48 days of growth. The model represents root morphology at the local rhizosphere scale, including root hairs and fine S-type laterals. It simulates fast- and slowly reacting soil P and the P-solubilizing effect of root-induced pH changes in the soil. Simulations predict that the zone of pH changes and P solubilization around a root spreads further into the soil than the zone of P depletion. A root needs to place laterals outside its depletion- but inside its solubilization zone to maximize P uptake. S-type laterals, which are short but hairy, appear to be the key root structures to achieve that. Thus, thicker roots facilitate the P uptake by fine lateral roots. Uptake can be enhanced through longer root hairs and greater root length density but was less sensitive to total root length and root class proportions.

KEYWORDS
Rhizosphere pH; slow sorption; coupled transport model; phosphorus uptake efficiency

1 | INTRODUCTION

Deficiency of phosphorus (P) is one of the main constraints to crop production on highly weathered soils of the humid tropics (Alewell et al., 2020). Owing to the high content of iron and aluminum oxides in the clay fractions of such soils, added P becomes strongly sorbed on soil surfaces and is therefore largely unavailable to plant roots. However, certain plant species – exemplified by upland rice (*Oryza sativa*) – are efficient in extracting this strongly sorbed P. There are large differences in tolerance of low P availability in the upland rice germplasm (Rose et al., 2013; Vandamme et al., 2016) and there has been progress in mapping the associated genes (Gamuyao et al., 2012; Schatz et al., 2014; Mori et al., 2016). However, the mechanisms involved are poorly understood (Nestler and Wissuwa, 2016; Wissuwa et al., 2020). Genotypes differ in total P uptake, P uptake per unit root surface area, and biomass per amount of P taken up – i. e. the internal P use efficiency (Wissuwa et al., 2015, 2020). Mathematical models are needed to describe the underlying mechanisms. In this paper, we develop such a model, focusing on the processes involved in P uptake.

Four factors potentially influence plant P uptake and need to be considered: (1) root length, diameter, architecture, and coverage with hairs, as these affect the surface area available for P uptake; (2) the P uptake per unit surface area of roots and hairs; (3) root-induced changes in the soil that affect the solubility of P; and (4) the effects of rhizosphere microbes and mycorrhizal fungi. Current understanding of these factors for upland rice is as follows.

First, root architecture and morphology. The upland rice root system comprises large numbers of roots which are classified into crown, seminal, L-type and S-type lateral roots. S-types are short and fine lateral roots (<1 cm length; <80 µm diameter) unique to rice (Yamauchi et al., 1987) and typically double the total length of a root system (Kant et al., 2018; Wissuwa et al., 2020). The crown and lateral roots, including the fine S-types, produce hairs. Recent 3D modeling, allowing for soil transport, uptake limitations, S-type lateral roots, and hairs, shows that the P cost of those fine laterals is recovered within a day of their formation (Gonzalez et al., 2021). They are therefore efficient in the use of P.

Second, the P uptake per unit root surface area. Conventional models of P uptake treat individual roots as

'sinks' to which P is delivered by transport through the soil solution (Kuppe et al., 2021b). The sink strength is modeled as function of P concentration in solution at the root surface and the activity of P uptake transporters in the root membrane. Such models greatly under-predict P uptake by upland rice grown in strongly P-sorbing soils, both when root architecture is (Gonzalez et al., 2021; De Bauw et al., 2020) and is not considered (Kirk et al., 1999). In strongly sorbing soils, P concentrations in the soil solution can be so low that even high-affinity transporters may still be slow in taking it up. Rates of transport through the soil by diffusion are, however, even slower (note rates of mass flow in the transpiration stream are negligible at these P concentrations). The conventional models underestimate P uptake even when it is assumed that the root reduces the P concentration at its surface to zero. This suggests that other processes, not allowed for in the conventional models, are important.

Third, root-induced solubilization. Solubilization of P through the secretion of low molecular weight organic acid anions, such as citrate and malate, is widely discussed (Hinsinger et al., 2011; Oburger et al., 2009; Hoffland, 1992). For rice, Kirk et al. (1999) used a model developed by Kirk (1999) and calculated the rates of citrate secretion from roots required to explain the measured rates of P uptake. The P-solubilizing effect of citrate and the rate of citrate decomposition were determined experimentally. However, the measured effluxes of citrate and other P-solubilizing organic exudates from rice roots (Wissuwa, 2005) are much smaller than required. Likewise, there is no evidence for organic P solubilization by release of phosphate enzymes from upland rice roots (Hedley et al., 1994) or genotypic differences in phosphatase secretion (Rakotoson et al., 2020). We, therefore, exclude the role of organic acids or phosphatases in P uptake.

A further potential solubilization mechanism is by root-induced pH changes in the soil. Roots that take up nitrogen as nitrate (NO_3^-) tend to take up an excess of anions over cations, balanced by the release of bicarbonate (HCO_3^-) anions, so causing an increase in rhizosphere pH (Nye, 1981; Dijkshoorn et al., 1968). In soils with pH-dependent surface charge, an increase in pH tends to make the surface charge more negative and less P-sorbing (Barrow, 2017; Penn and Camberato, 2019). Hence, P becomes more plant available.

Fourth, mycorrhizal fungi and effects of the rhizosphere microbiome. Wissuwa et al. (2020) assessed the effects of mycorrhizal colonization on P uptake by P-efficient and -inefficient genotypes of upland rice in

strongly P-sorbing soil. Differences in mycorrhizal colonization – and expression of a mycorrhiza-induced P transporter (OsPT11) confirming that the symbiosis was functional – could not explain the genotypic variation in uptake per unit root surface area. Efficient genotypes always out-performed inefficient ones, independent of soil sterilization and inoculation treatments. This indicates that plant-specific factors rather than mycorrhizal fungi or other soil microbiome effects were responsible for the greater root efficiency. Though free-living microbes may solubilize P to some extent, there is little known to build a model, and any P solubilized at a distance from a root must get to a root surface.

To quantify the importance of these various factors for P acquisition by upland rice, we developed a new rhizosphere model and a method for up-scaling to the whole plant, and tested it against experimental data. This is the first published model to allow for interaction between root morphology and root-induced solubilization processes. We use it to ask (1) if solubilization by pH changes can quantitatively explain the measured P uptake of genotype DJ123; (2) how sensitive P uptake would be to variations in root and soil parameters, and thereby how root morphology contributes to P uptake; and (3) how much the individual root classes contribute to uptake, particularly the metabolically cheap S-types.

2 | MATERIALS AND METHODS

We simulate uptake of P and efflux of HCO_3^- over root surfaces based on diffusion-reaction equations radially symmetrical to the root axis (Figure 1a). The HCO_3^- balances excess intake of nutrient anions over cations due to plant nutrient demand. Reaction of HCO_3^- with the soil increases the soil pH and the concentration of P in the soil solution.

The total P in the system is the sum of P in the soil solution, P in the soil solid, and P taken up. The soil solid P is conceptually divided into pools that differ in their sorption and solubilization rates. Increasing pH leads to a faster desorption and a fast solubilization of P (Figure 1b).

We distinguish three root classes characteristic of rice: the crown roots, (long) L-type laterals, and

(short) S-type laterals, all with hairs (Figure 1a). We include seminal roots with the crown roots because the distinction is experimentally difficult in older plants. The uptake by unit length of L-type laterals and crown roots, both including their S-type lateral branches, are scaled-up to the whole root system using a fitted root growth function (section 2.3). The S-type laterals are treated as sink and source terms in the rhizosphere of a crown root and L-type lateral.

We assume P has a negligible influence on HCO_3^- because the amount of HCO_3^- reacting is much larger than the amount of P in solution. Therefore, we first describe the equation for movement of HCO_3^- and resulting pH changes because it is formulated independently of P. Secondly, we describe the equations for pH-dependent P diffusion and reaction, including P uptake by root hairs, S-type laterals, and hairs of S-type laterals. Thirdly, we describe the upscaling of the rhizosphere model to the total root system. Main symbols are defined in Table 1.

[Figure 1 about here]

[Table 1 about here]

2.1 | HCO_3^- efflux and diffusion

The pH increase, resulting from the reaction of HCO_3^-, is propagated away from the root surface by acid-base transfer (Nye, 1981). The dominant acid-base pairs are H_3O^+—H_2O and H_2CO_3—HCO_3^-, the latter formed by equilibration with CO_2 in the soil air. The corresponding continuity equation for the concentration of titratable soil acidity, HS, is (after Nye, 1981)

$$\frac{\partial HS}{\partial t} = \frac{1}{r}\frac{\partial}{\partial r}\left(r\theta f\left(D_H\frac{\partial H_\ell}{\partial r} - D_B\frac{\partial B_\ell}{\partial r}\right)\right) + E_\mathrm{R}, \tag{1}$$

where H_ℓ, B_ℓ are concentrations in soil solution, D_H, D_B are diffusion constants in water for H_3O^+ and HCO_3^-, respectively, θ is the volumetric water content, and f is the diffusion impedance factor. The reaction term $E_R(r,t)$ is the efflux out of root hairs, S-types, and S-type hairs into the rhizosphere. The efflux of HCO_3^- over the whole root system balances the excess intake of anions (NO_3^-, $H_2PO_4^-$, SO_4^{2-}) over cations (NH_4^+, K^+, Ca^{2+}, Mg_2^+). We assume a constant efflux (E) per unit root surface area over all root classes. We express HS in terms of B_ℓ as follows. Changes in HS are related to changes in pH by the soil pH buffer power, b_{HS}, defined as $b_{\mathrm{HS}} = -d\,HS/d\mathrm{pH}$. From $\mathrm{pH} = -\ln H_\ell / \ln 10$ and $d\,H_\ell/H_\ell = -d\,B_\ell/B_\ell$, we get $d\,HS = -b_{\mathrm{HS}} d\,B_\ell/(B_\ell \ln 10)$. Also $d\,H_\ell = -K/B_\ell^2\, d\,B_\ell$, with $B_\ell = K/H_\ell$, and abbreviation defined as $K = K_1 K_s p_{CO_2}$, where K_1 is the first apparent dissociation constant of H_2CO_3, K_s is the solubility of CO_2 in water, and p_{CO_2} the CO_2 pressure in the soil air. Thereby we obtain

$$\frac{\partial B_\ell}{\partial t} = \frac{B_\ell \ln 10}{b_{\mathrm{HS}}} \left[\frac{1}{r} \frac{\partial}{\partial r} \left(r\theta f \left(\frac{D_H K}{B_\ell^2} + D_B \right) \frac{\partial B_\ell}{\partial r} \right) + E_R \right]. \tag{2}$$

Note that $b_{\mathrm{HS}} / \left(B_\ell \ln 10 \right)$ in Eqn 2 is the soil buffer power for HCO_3^-, which varies inversely with B_ℓ.

The boundary condition at $r = r_0$ is

$$\theta f \left(\frac{D_H K}{\left(B_\ell(r_0,t) \right)^2} + D_B \right) \frac{\partial B_\ell(r_0,t)}{\partial r} = -E. \tag{3}$$

The zero-flux boundary condition at the rhizosphere outer radius, $r = r_1$, is

$$\frac{\partial B_\ell(r_1,t)}{\partial r} = 0. \tag{4}$$

We assume the initial pH throughout the soil around the root is constant at $t = 0$; initial condition $B_\ell(r, 0) = B_{\ell,\text{init}}$.

2.2 | P diffusion, reaction, and uptake

The rate of change in P concentration in the soil is

$$\frac{\partial P}{\partial t} = \theta \frac{\partial P_\ell}{\partial t} + \rho \left(\frac{\partial P_{s,\text{fast}}}{\partial t} + \frac{\partial P_{s,\text{fast-sol}}}{\partial t} + \frac{\partial P_{s,\text{slow}}}{\partial t} \right), \tag{5}$$

where P_ℓ is the P concentration in the soil solution, $P_{s,\text{fast}}$ is the concentration in rapid equilibrium with the soil solution at the initial pH, $P_{s,\text{fast-sol}}$ is the concentration of P rapidly solubilized as the pH is increased, and $P_{s,\text{slow}}$ is the concentration in slow equilibrium. The relation between $P_{s,\text{fast}}$ and P_ℓ is defined by the soil P buffer power $b_\text{P} = \theta + \rho \left(\partial P_{s,\text{fast}} / \partial P_\ell \right)_{B_\ell}$, and the additional P solubilized as the the pH increases is obtained by introducing a P-HCO_3^- interaction coefficient, $\lambda = \left(\partial P_\ell / \partial B_\ell \right)_P$ (after Nye, 1983). Note, b_P and λ are defined at constant concentrations of HCO_3^- and P in the whole soil, respectively. The equations for slow P sorption and its dependence on P_ℓ and B_ℓ are given in section 2.2.1. Substitution and rearranging of Eqn 5 gives

$$\frac{\partial P}{\partial t} = b_\text{P} \left(\frac{\partial P_\ell}{\partial t} - \lambda \frac{\partial B_\ell}{\partial t} \right) + g \tag{6}$$

where $g = \rho \partial P_{s,\text{slow}} / \partial t$ (see Supporting Information).

Now consider the change of P concentration around a crown root or L-type lateral as continuity equation

for P diffusion

$$\frac{\partial P}{\partial t} = \frac{1}{r}\frac{\partial}{\partial r}\left(r D_P \theta f \frac{\partial P_\ell}{\partial r}\right) - I_\mathrm{R} \tag{7}$$

where I_R is the rate of uptake inside the rhizosphere domain by the S-type lateral surfaces (I_S) and the hairs on the S-types (I_hS) and parent root (I_h), i. e. $I_\mathrm{R} = I_\mathrm{h} + I_\mathrm{S} + I_\mathrm{hS}$. Combining Eqns 6 and 7 and rearranging gives

$$\frac{\partial P_\ell}{\partial t} = \frac{1}{b_\mathrm{P}}\left[\frac{1}{r}\frac{\partial}{\partial r}\left(r D_P \theta f \frac{\partial P_\ell}{\partial r}\right) - I_\mathrm{R} - g\right] + \lambda \frac{\partial B_\ell}{\partial t} \tag{8}$$

The influx into the crown root or L-type lateral at $r = r_0$ is given by Michaelis-Menten kinetics with the same V_max and K_m for each root class. There is no flux of P across the boundary $r = r_1$ between the zones of influences of neighboring roots, and the initial P concentration is uniform throughout the soil. Hence,

$$D_P \theta f \frac{\partial P_\ell(r_0, t)}{\partial r} = \frac{V_\mathrm{max} P_\ell(r_0, t)}{K_\mathrm{m} + P_\ell(r_0, t)}, \tag{9}$$

$$\frac{\partial P_\ell(r_1, t)}{\partial r} = 0, \tag{10}$$

$$P_\ell(r, 0) = P_{\ell,\mathrm{init}}. \tag{11}$$

2.2.1 | Slow P sorption

In measurements of P desorption, there is generally an initial rapid release followed by a much slower release, which may continue for days or longer (Barrow, 2008). We describe this slow reaction and its dependence on

pH as

$$\rho \frac{\partial P_{s,\text{slow}}}{\partial t} = \kappa_a \, \theta \, P_\ell - \kappa_d \, \rho P_{s,\text{slow}}, \tag{12}$$

where κ_a and κ_d are functions of B_ℓ. Note, the notation for the r, t-dependency of variables is dropped to improve readability. We allow for the effect of pH on the slow sorption rates with

$$\kappa_a = k_1 - k_1^* \left(B_\ell - B_{\ell,\text{init}} \right), \tag{13}$$

$$\kappa_d = k_2 + k_2^* \left(B_\ell - B_{\ell,\text{init}} \right), \tag{14}$$

where k_1^*, k_2^* are additional adsorption and desorption rate constants. Hence, an increase in B_ℓ results in increased P release from slowly reacting P.

2.2.2 | Root hairs and S-type laterals

The root hairs and S-type laterals are inside the rhizosphere of their parent roots (Figure 1a) and are therefore sink terms for P in Eqn 8 and source terms for HCO_3^- in Eqn 2. Starting with uptake by hairs and S-types, we calculate influx by assuming steady-state diffusion across their depletion zones following Baldwin et al. (1973), Bhat et al. (1976), Itoh and Barber (1983a) as justified by Leitner et al. (2010), and formulated for numerical discretizations by Kuppe et al. (2021a).

The equations for root hairs are as follows (S-types and their hairs are in the Supporting Information).

The rate of uptake by hairs per unit soil volume at distance r from the parent root is

$$I_\mathrm{h} = \frac{V_\mathrm{max} P_\mathrm{rh}}{K_\mathrm{m} + P_\mathrm{rh}} A_\mathrm{h}, \tag{15}$$

where P_rh is the concentration in solution at the root hair surface, A_h is the surface area of hairs per unit soil volume, and V_max and K_m are Michaelis-Menten constants, which, we assume, have the same values for root and hairs. The value of A_h over an interval dr along the root hair length is given by (Kuppe et al., 2021a, Eqn 5)

$$A_\mathrm{h} = \begin{cases} \frac{2 r_\mathrm{h} N_\mathrm{h} \mathrm{d}r}{(r+\mathrm{d}r)^2 - r^2} & \text{for } r < l_\mathrm{h} + r_0 \\ 0 & \text{for } r \geq l_\mathrm{h} + r_0. \end{cases} \tag{16}$$

where r_h and l_h are the radius and length of root hairs, respectively, and N_h is the number of hairs per unit hair length.

The mean P concentration in solution in the depletion zone around a hair is (after Baldwin et al., 1973, Eqn iii)

$$\overline{P_\ell} = P_\mathrm{rh} + \frac{r_\mathrm{h} \cdot V}{D_P \theta f} \left(\frac{{r_\mathrm{h1}}^2}{{r_\mathrm{h1}}^2 - {r_\mathrm{h}}^2} \ln\left(\frac{r_\mathrm{h1}}{r_\mathrm{h}}\right) - \frac{1}{2} \right), \tag{17}$$

where the uptake V is a function of P_rh. Substituting $V(P_\mathrm{rh}) = V_\mathrm{max} P_\mathrm{rh} / (K_\mathrm{m} + P_\mathrm{rh})$, rearranging and solving

the resulting quadratic equation gives

$$P_{rh} = \frac{1}{2}\left(\overline{P_\ell} - K_\mathrm{m} - \varphi + \sqrt{\varphi^2 + 2\varphi(K_\mathrm{m} - \overline{P_\ell}) + (K_\mathrm{m} + \overline{P_\ell})^2}\right) \tag{18}$$

where $\varphi = \frac{r_\mathrm{h} V_\mathrm{max}}{D_P \theta f}\left(\frac{{r_\mathrm{h1}}^2}{{r_\mathrm{h1}}^2 - {r_\mathrm{h}}^2} \ln\left(\frac{r_\mathrm{h1}}{r_\mathrm{h}}\right) - \frac{1}{2}\right)$. This estimating of P_rh accounts for root hair depletion, remembering $P_\mathrm{rh} < P_\ell$. The mean concentration in the depletion zone around the hair ($\overline{P_\ell}$) at distance r from the parent root is equal to P_ℓ in the numerical solution of Eqn 8. Hence, P_ℓ in Eqn 18, the steady-state, is updated at each time-point t. The mid-point between adjacent hairs at distance r is $r_\mathrm{h1} = \sqrt{r\pi/(2N_\mathrm{h})}$.

The radius of S-type laterals is so small that we can treat the S-types as sink terms in Eqn 8 in the same way as we do for root hairs. The corresponding equations are in the Supporting Information. The length of S-types per unit length of crown root or L-type is

$$L_\mathrm{SR} = \frac{\omega_\mathrm{S}}{\omega_\mathrm{L} + \omega_\mathrm{C}}. \tag{19}$$

We assume that L_SR [cm cm^{-1}] is constant over time and the S-type density is the same for crown roots and L-type laterals. The actual S-type length in the rhizosphere is $L_\mathrm{S,act} = r_1 - r_0$, which increases the number of S-types per cm root according to L_SR.

Given the surface areas densities A_h [cm^2 cm^{-3}], Eqn 16, $A_\mathrm{S,surf}$, and $A_\mathrm{S,hairs}$ (see Supporting Information), the reaction term in Eqn 2 for efflux into the rhizosphere is $E_\mathrm{R}(r,t) = -E(A_\mathrm{h} + A_\mathrm{S,surf} + A_\mathrm{S,hairs})$.

2.3 | Uptake rate per segment and upscaling to the whole root system

The cumulative uptake per unit root length of each class (L-type or crown root) at time t,

$$U(t) = \int_0^t \dot{U}(s) ds,$$

is the sum of the uptake by the root and its hairs,

$$U = U_{\text{hairs}} + U_{\text{surf}} + U_{\text{S,surf}} + U_{\text{S,hairs}} \tag{20}$$

with corresponding uptake rates of P over time per unit root length, for root hairs

$$\dot{U}_{\text{hairs}}(t) = 2\pi r_{\text{h}} N_{\text{h}} \int_{r_0}^{r_0+l_{\text{h}}} \frac{V_{\max} P_{\text{rh}}}{K_{\text{m}} + P_{\text{rh}}} dr \tag{21}$$

which we calculate by summing the volumetric I_h of Eqn 15 corrected to area, and the root surface

$$\dot{U}_{\text{surf}}(t) = 2\pi r_0 \frac{V_{\max} P_{\ell}(r_0, t)}{K_{\text{m}} + P_{\ell}(r_0, t)}. \tag{22}$$

The rates of uptake by the surfaces and hairs of S-types are found with analogous equations.

We are interested in uptake by whole root systems, not just root segments. Scaling up to the whole root system requires that we take the age distribution of the roots into account. Therefore, we define the time

derivative $\dot{L}(t)$ of a function of the total root length $L(t)$. The total P uptake is

$$\mathcal{P}(t) = \int_0^t \dot{L}(s) U(t-s) ds, \tag{23}$$

where $dL = \dot{L}(s)ds$, here, $t \leq t_{\text{end}} = 48\,\text{d}$. The root system P uptake is the sum of uptake for each class (Supporting Information).

We assume that the crown and lateral roots experience the same initial soil conditions everywhere in the soil. For the default simulation, we assume proportions of root class length to be constant over time. For the sensitivity analysis, we allow for change in length of root classes and their proportions, following Wissuwa et al. (2020), however, constant over time.

2.4 | Numerical solution and mass balance

Eqns 2, 8, and 12 were solved subject to their initial and boundary conditions using a higher-order numerical method (details in Supporting Information). The relative mass balance error of P in the system was in the order of 10^{-5}. The sum of the amount of P taken up by the plant and that remaining in the soil per unit root length at any time is given by

$$M_{\text{sum}} = M_{\ell} + M_{s,\text{fast}} + M_{s,\text{fast-sol}} + M_{s,\text{slow}} + U \tag{24}$$

where U is the plant uptake per unit root length (Eqn 20) and M_{ℓ}, $M_{s,\text{fast}}$, $M_{s,\text{fast-sol}}$, $M_{s,\text{slow}}$ are the amounts of P in the soil volume influenced by the root per unit root length at time t, subscripted as for the P concentrations in the soil (Eqn 8).

2.5 | Plant parameters

2.5.1 | Measurements

Wissuwa et al. (2020) measured time courses of root growth and P uptake by rice genotype DJ123 (which is considered efficient in P uptake, Mori et al., 2016) grown on a strongly P-sorbing volcanic ash soil with low available P (Andosol) in Tsukuba, Japan. Plants were grown in a field under aerobic upland conditions or in large 72-L boxes filled with the low-P Andosol from that same field. Entire root systems were collected at 7, 14, 21, and 28 days after emergence (DAE) from the box, and at 16, 28, and 48 DAE from the field. Root system excavation in the field was limited to a depth of 30 cm, which typically contains > 90 % of entire root biomass in rice (Mori et al., 2016). Roots were scanned and analyzed using the WinRHIZO software, with diameter settings of 0–0.009 cm, 0.009–0.025 cm and 0.025–0.1 cm for S-type, L-type, and crown roots, respectively. By 28 DAE the roots in boxes were too large to be scanned and total root length was estimated based on root dry weight and conversion factors determined from previous scans. Shoot samples were taken at the same times as roots, and P concentrations in shoot and root were determined to calculate the quantity of P taken up. The box experiment was repeated in June 2019.

Nestler and Wissuwa (2016) measured the length and densities of the root classes and their coverage with hairs in genotype DJ123 under the conditions as the Wissuwa et al. (2020) field experiment (Table 2). Plants were grown in the field and, at 50 days after seeding, a 1 m deep trench was dug perpendicular to the plant rows across the field to sample the roots. Intact roots were removed by washing and stored at 4 °C in 50 % ethanol prior to root hair evaluation. Using the longest crown root of a plant, 1 cm long sections at 1, 10, 15, 20, and 25 cm from the root tip were imaged to determine root hair length and density on the crown root and its laterals as described by Nestler et al. (2016).

2.5.2 | Root length, S-type length, and RLD

To the measured root length, we fitted the function

$$L(t) = \frac{a \exp(t)}{(c + \exp(t))^b} \tag{25}$$

with parameters a, b, and c using least square means, as shown in Figure 2a. This function is able to fit the experimentally observed growth jump after day 7.

Half the total length of the root system was S-type laterals ($\omega_S = 0.5$, Table 2), and we assume an equal proportion of S-types for crown roots and L-type laterals over time. Therefore, the S-type length per segment from Eqn 19 is $L_{SR} = 1\,\mathrm{cm\,cm^{-1}}$ for both classes of parent root.

The root length density (RLD) is calculated by dividing the total root system length of roots ($2.5 \times 10^4\,\mathrm{cm\,plant^{-1}}$) by a nominal rooted soil volume in the experiments based on the plant spacing ($10\,\mathrm{cm} \times 15\,\mathrm{cm\,plant^{-1}}$) and rooting depth (30 cm), giving RLD = $5.55\,\mathrm{cm\,cm^{-3}}$. The mean radial mid-point between adjacent crown roots or L-type laterals is therefore

$$r_1 = \sqrt{\frac{1 + L_{SR}}{\mathrm{RLD} \cdot \pi}} = 0.34\,\mathrm{cm}. \tag{26}$$

2.5.3 | Root P uptake kinetics and HCO_3^- efflux

We set the values of the Michaelis-Menten coefficients for P uptake such that they are not limiting, i. e. the concentration in solution at the root surfaces was reduced to near zero and uptake was not sensitive to increases in V_{max} or decreases in K_m. The values for all root classes were $V_{max} = 8 \times 10^{-12}\,\mathrm{mol\,cm^{-2}\,s^{-1}}$ and $K_m = 1 \times 10^{-9}\,\mathrm{mol\,cm^{-3}}$.

Given that the P concentrations in soil solution are very low, the influx depends on the initial slope of the function $V(P_\ell) = V_{\max} P_\ell / (K_m + P_\ell)$. For $K_m \gg P_\ell$ or $P_\ell \to 0$, the ratio of $V_{\max}$ and K_m gives, approximately, the relevant slope. We discuss root P uptake properties further in Section 4.3.

In principle, the HCO_3^- efflux per unit root surface area, E, may vary with differences in cation and anion intake over the root system. However, to avoid undue complexity, we used a constant value across the root system based on the measured plant growth and nutrient intakes. The upscaled HCO_3^- efflux (as described in section 2.3 for uptake) fitted the data well ($R^2 = 0.93$). Consider the increase in shoot and root dry weight of approximately 4.5 g plant^{-1} and the mean root surface area of 1.25×10^4 cm^2 between 28 and 48 DAE (Wissuwa et al., 2020). We used the following typical nutrient contents for rice during vegetative growth (Dobermann and Fairhurst, 2000): N, K, Ca, Mg, S were 30, 20, 3, 2, 2 mg g^{-1}, respectively; and measured P content of 1 mg g^{-1}. Assuming all the N was taken up as NO_3^-, which is reasonable because nitrification is rapid in this soil under the conditions of the experiment (Nardi et al., 2013), the uptake of cations (K^+, Ca^{2+}, Mg^{2+}) was 3.96 mol plant^{-1} and that of anions (NO_3^-, $H_2PO_4^-$, SO_4^{2-}) was 10.66 mmol plant^{-1}, which is an anion excess of 6.7 mmol plant^{-1}. Dividing this by the time-integral of root surface area gives the efflux rate $E = 1.83 \times 10^{-12}$ mol cm^{-2} s^{-1}.

[Table 2 about here]

2.6 | Soil parameters

2.6.1 | Measurements

The basic soil properties were clay = 17 %, silt = 43 %, organic C = 4.7 % and pH (1:5 H_2O) = 5.8. From the experimental set up: $\rho = 0.87$ g cm^{-3} and $\theta = 0.3$. The diffusion impedance factor at the given bulk density and moisture content, $f = 0.24$, was measured by following the diffusion of a trace amount of non-adsorbed Br^- applied on one end of a block of the soil by the method of Darmovzalova et al. (2020).

We measured the initial P concentration in the soil solution, $P_{\ell,\text{init}}$, as follows. Portions (120 g) of

air-dry soil were moistened to 50 % of field capacity with deionized water and incubated in sealed containers at approximately 20 °C for 21 d. The moist soil was then centrifuged and the supernatant filtered through 0.45 µm filters (Whatman). Filtered supernatant (approximately 30 cm^3) was shaken with a DGT device (DGT Research Ltd, UK) for 24 h, and the P adsorbed on the DGT ferrihydrite gel was desorbed into 1 cm^3 of 1 M HCl for 24 h, and measured colorimetrically.

We estimated the other soil P fractions using the Hedley et al. (1982) sequential fractionation scheme (Table 3). Samples (1.0 g) of oven-dry soil were extracted sequentially for 16 h each with (1) a strip of HCO_3^--form anion exchange resin membrane (adsorption capacity 26 µmol per strip) in H_2O, recovering P from the resin by extraction in 0.5 M HCl; (2) 30 cm^3 of 0.5 M $NaHCO_3$, followed by digestion in H_2SO_4 and H_2O_2; (3) 30 cm^3 of 0.1 M NaOH, followed by digestion of the extract in H_2SO_4 and H_2O_2; and (d) 30 cm^3 of 1 M HCl; and finally (4) by digestion of the residual soil in H_2SO_4 and H_2O_2. Total P in the $NaHCO_3$ and NaOH extracts was obtained from P in the digested extract and organic P (P_o) was inferred from the total P less the inorganic P (P_i) measured in the undigested extracts. P concentrations in the extracts were measured colorimetrically by the molybdenum blue method (Murphy and Riley, 1962).

The pH buffer capacity (soil pH buffer power), b_{HS}, was measured by shaking 2 g portions of the soil in 10 cm^3 of 10 mM $CaCl_2$ overnight with sufficient NaOH to raise the final pH by approximately 1 pH-unit. This gives $b_{HS} = 1 \times 10^{-5}$ mol cm^{-3} (pH unit)$^{-1}$ (see also Nye, 1981). We take a typical value for CO_2 pressure in the soil air, $p_{CO_2} = 4 \times 10^{-3}$ atm (Figure 1 in Nye, 1981).

[Table 2 about here]

2.6.2 | Soil P pools

Following Hedley et al. (1994), who measured depletion of NaOH-P_i by upland rice, we define the total concentration of P that is ultimately available for uptake by a root as

$$P = \theta P_\ell + \rho \left([\text{Resin-P}] + [\text{NaHCO}_3\text{-P}_i] + [\text{NaOH-P}_i] \right) \tag{27}$$

We assume [Resin-P] and [$NaHCO_3$-P_i] are in rapid equilibrium with the soil solution, and an additional proportion α of [NaOH-P_i] is rapidly released if the pH is raised by one unit. Hence, the initial values of $P_{s,\text{fast}}$ and $P_{s,\text{fast-sol}}$ are

$$P_{s,\text{fast}} = [\text{Resin-P}] + [\text{NaHCO}_3\text{-P}_i] \tag{28}$$

$$P_{s,\text{fast-sol}} = \alpha [\text{NaOH-P}_i] \tag{29}$$

The component of [NaOH-P_i] that slowly equilibrates at the initial pH is

$$P_{s,\text{slow}} = (1 - \alpha) [\text{NaOH-P}_i]. \tag{30}$$

If the soil pH is raised by one unit and allowed to equilibrate, the new mass balance of P is

$$P = b_\text{P} P^*_\ell + \rho P^*_{\text{s,slow}} \tag{31}$$

where

$$\beta = \frac{P^*_{\text{s,slow}}}{P_{\text{s,slow}}} \tag{32}$$

and $P^*_{\text{s,slow}}$, P^*_ℓ are the equilibrium concentrations at pH = $\text{pH}_{\text{initial}} + 1$. The coefficients α and β are both less than one and pre-set. We used values $\alpha = 0.33$ and $\beta = 0.4$. Substituting the measured Hedley fractions (Table 3) and $P_\ell = 8 \times 10^{-11}\,\text{mol}\,\text{cm}^{-3}$ at the initial pH in Eqn 27 and 31 gives $P^*_\ell = 1.4 \times 10^{-9}\,\text{mol}\,\text{cm}^{-3}$.

2.6.3 | P soil buffer power and P-HCO_3^- interaction coefficient

We estimate the soil buffer power, $b_\text{P} = \left(\partial P_\text{e}/\partial P_\ell\right)_{B_\ell}$, from $b_\text{P} = \theta + \rho\left(P_{s,\text{fast}}/P_\ell\right)_{\text{initial}}$, note $\theta \ll b_\text{P}$ and $P_\text{e} = \theta P_\ell + \rho\left(P_{s,\text{fast}} + P_{s,\text{fast-sol}}\right)$, $\partial P_{s,\text{fast-sol}}/\partial P_\ell = 0$. Substituting $P_{\ell,\text{init}} = 0.08\,\mu\text{M}$, $P_{s,\text{fast}} = 0.5\,\mu\text{mol}\,\text{g}^{-1}$, and $\rho = 0.87\,\text{g}\,\text{cm}^{-3}$ gives $b_\text{P} \approx 5440$.

We estimate the P-HCO_3^- interaction coefficient, λ, as follows. If ΔP_e is the change required to leave P_ℓ unchanged following unit increase in pH above the initial pH, then (following Nye, 1983):

$$\Delta P_\ell = \left(\frac{\partial P_\ell}{\partial P_\text{e}}\right)_{B_\ell} \Delta P_\text{e} + \left(\frac{\partial P_\ell}{\partial B_\ell}\right)_P \Delta B^*_\ell = 0. \tag{33}$$

Substituting $b_\text{P} = \left(\partial P_\text{e}/\partial P_\ell\right)_{B_\ell}$ and $\lambda = \left(\partial P_\ell/\partial B_\ell\right)_P$ and rearranging gives

$$\lambda = \frac{\rho P_{s,\text{fast-sol}}}{b_\text{P}\Delta B^*_\ell} \tag{34}$$

where ΔB^*_ℓ is the change in B_ℓ for unit increase in pH above the initial value. This gives $\lambda = 1.49 \times 10^{-3}$.

2.6.4 | Adsorption-desorption rates

The half-times of slow equilibration, obtained by integrating Eqn 12 at constant P_ℓ, are

$$t_{1/2} = \frac{\ln 2}{k_2} \tag{35}$$

$$t^*_{1/2} = \frac{\ln 2}{k_2 + k^*_2 \Delta B^*_\ell}. \tag{36}$$

The half-times for strongly P-sorbing soils are in the order of weeks (Barrow, 2008). Hence, we obtain $k_2 = 2.87 \times 10^{-7}\ \mathrm{s}^{-1}$ and $k^*_2 = 9.31\ \mathrm{cm}^3\ \mathrm{mol}^{-1}\ \mathrm{s}^{-1}$ for trial values $t_{1/2} = 28\ \mathrm{d}$, $t^*_{1/2} = 2\ \mathrm{d}$ after unit pH change, respectively. We then compute k_1 and k^*_1 from the following equations. At equilibrium, $\partial P_{s,\mathrm{slow}}/\partial t = 0$, and so from Eqns 12–14,

$$k_1 \theta P_{\ell,\mathrm{init}} = k_2 \rho P_{s,\mathrm{slow}} \tag{37}$$

$$\left(k_1 - k^*_1 \Delta B^*_\ell\right) \theta P^*_\ell = \left(k_2 + k^*_2 \Delta B^*_\ell\right) \rho \beta P_{\mathrm{s,slow}}, \tag{38}$$

where ΔB^*_ℓ is the change in B_ℓ for unit increase in pH above the initial value. Substituting the above values in these equations gives $k_1 = 7.86 \times 10^{-2}\ \mathrm{s}^{-1}$ and $k^*_1 = 1.34 \times 10^5\ \mathrm{cm}^3\ \mathrm{mol}^{-1}\ \mathrm{s}^{-1}$.

[Table 3 about here]

2.7 | Simulations and sensitivity analysis

Uptake from the rhizospheres of unit length crown roots and L-type laterals are simulated over a 48 d growth period and upscaled with the method described in section 2.3. The default parameters, Table 4, are used as a reference parameter set in the sensitivity analysis. The parameters are varied relative to their default value over a four-fold change.

Scaling of the rates for efflux

We assume the same total amount of HCO_3^- released for varying root morphological traits. The amount of HCO_3^- released depends on the surface area of the root system and the efflux integrated over time. For parameters that change the root surface area, we scale the efflux per unit root surface area (E), so that the HCO_3^- released by the whole root system remains unchanged (Supporting Information, Figure S1: upscaled segment efflux). Also, the efflux, E, is varied in a range that does not increase pH more than one unit locally (as the model is limited by $\Delta B_\ell = 4 \times 10^{-7}$ mol cm^{-3}, which is approx. ΔpH = 1.06). Here, the variation of efflux with fixed default root size can be interpreted as a change in total nutrient uptake, i. e. the balance between cation and anion uptake.

Distances to neighboring roots

Changing the outer radius, r_1, from half to double, other parameters fixed (in particular $L_{\mathrm{SR}} = 1$), the RLD changes in a range from 1.39 to 22.2 cm cm^{-3} (eight-fold for RLD). Placing main root segments closer together by reducing the outer radius also decreases the distances among S-type laterals. The mid-distance to the neighboring root, r_1, does not influence the efflux, but the pH change can drastically increase when the distance to the zero-flux outer boundary decreases. Thus HCO_3^- accumulates when the volume of the rhizosphere decreases and the RLD increases. The variation of the outer radius (measured from the center of the root) is limited to unit pH change and, thereby, uptake was not simulated for $r_1 < 0.3386$ for crown roots.

Root length

S-type length is changed via L_{SR} (Eqn 19, change in ω_S fixed ω_L and ω_C) and with this, RLD changes (max. 8.33 for $2 \cdot L_{SR}$). Note that L_{SR} determines the S-type number on a segment. The root length of crown roots and L-types is varied while keeping the default one cm S-type length per cm parent root and the number of root hairs per surface root area unchanged. Hence, a change in the length L_C, and L_L implies a change in total S-type length.

S-type proportion

We vary ω_S in Eqn 19 in order to vary L_{SR} while keeping either the root system length, the root surface area, or the root volume fixed. Note, L_{SR} changes $A_{S,surf}$ and $A_{S,hairs}$. We assume a fixed RLD and a fixed ratio of L-type by crown root proportion, ω_L/ω_C.

Solubilization fractions and rates

The total P in soil is kept constant for all simulations. We vary α, which partitioned the measured NaOH-P_i over $P_{s,slow}$ and $P_{s,fast\text{-}sol}$. We also vary the ad- and desorption rates and their responsiveness to the pH changes by varying the half-times of slow equilibration, $t_{1/2}$, $t^*_{1/2}$, for pH 5.8, 6.86, respectively, and β, Eqn 32. The half-times determine the desorption rates, k_2, k^*_2, whereas β determines the pH effect on the adsorption rate through a change in k^*_1.

3 | RESULTS

3.1 | Whole root system P uptake

Using the default parameter set (Table 4), we found that only 10 % of the observed uptake could be explained without allowing for solubilization, slow sorption, and S-types (Figure 2b). Including the S-type laterals and their root hairs as additional root-morphological features increased uptake significantly (2.6-times more than

without S-type laterals), but not sufficiently, the uptake was 26.4 % of that of the full model with solubilization, which fits the data. Allowing all of the NaOH-P_i to contribute to slow sorption without solubilization (i. e. making α in Eqns 29 and 30 equal to zero) increased P uptake, but only to 41 % of that with solubilization.

To simulate the measured uptake without solubilization and without slow sorption required either a 3.6-fold increase in $P_{\ell,\text{init}}$ or a 224-fold increase in $P_{s,\text{fast}}$ (Supporting Information, Figure S2). However, such a fast pool would lead to a soil-solution equilibrium constant, an order too high even when compared to whole inorganic solid phase P: $1.4 \times 10^6 \gg (P_{s,\text{fast}}(r, 0) + \text{NaOH-P}_i)/P_{\ell,\text{init}}$. Neither of these is plausible within the uncertainty of the parameter estimates.

3.2 | Importance of different root classes

Including hairs on respective root classes, crown roots took up 48.8 % of the total P compared to 30.6 % for S-type laterals and 20.6 % for L-type laterals (Figure 2c). The root hairs on S-types, L-types, and crown roots in sum were responsible for almost 77 % of the total uptake (black dashed line), where those on crown root and S-types mattered most with a combined uptake of approximately 64 % of the total. The results seem surprising, as it is generally thought that most P is taken up by lateral roots. This is still the case, but the lateral roots are here split over two classes: S- and L-types. To understand these results for the root system, we have to take a look at the cumulative uptake per unit length of crown and L-type lateral roots (Figure 3a vs. 3b).

[Figure 2 about here]

Cumulative uptake of P per unit root length by a crown root was 3.1-times that of an L-type lateral. This can be understood by considering that a crown root has three times the surface area per unit length with about double the number of root hairs. For crown roots, most of the uptake was achieved by the hairs of the crown root itself, whereas in the rhizosphere of L-type laterals, most of the uptake was by the root hairs on their S-type laterals. Very little was taken up over the S-type root surface. Hence, the root hair contribution to uptake increased when the main root radius decreased.

In models without solubilization, the P concentration is slowly depleted and the cumulative uptake levels off or becomes approximately linear since it only depends on the uptake from a buffered P solution. In our simulations, however, more P dissolved and the P uptake by S-type hairs increased exponentially over time (compare convex shape of dashed blue line versus concave shape of dashed cyan line in Figure 3a). Consequently, the cumulative uptake did not level off. The uptake rate even accelerated somewhat at later time points for S-type hairs while it slowed down sightly for crown root hairs. S-types by themselves did not achieve the necessary pH change (data not shown, separate uptake of S-types shown in Supporting Information, Figure S3), just like L-type laterals achieved a smaller pH change in their rhizosphere compared to crown roots. P uptake by S-type laterals depended on the efflux zone of the crown and L-type lateral roots, thereby on the parent root and on the proximity to other roots.

[Figure 3 about here]

3.3 | Rhizosphere P concentration profiles

Of importance to P-uptake is the concentration in the soil solution, P_ℓ, which is very small, but its dynamics follows $P_{s,\text{fast}}$ (Figures 3c and 3d). The spatial-temporal variation in P_ℓ (Figures 4a and 4b) shows that P_ℓ was quickly depleted close to the parent root surface. This depletion zone, however, was rather narrow (< 0.5 mm). For Figure 4, note that the root center is located at $r = 0$ and the root surface at $r = r_0$ (for crown roots $r_0 = 0.03$ and for L-type laterals $r_0 = 0.01$ cm, Table 2). P_ℓ was greatly increased one mm away from the root surface. The increase of up to ten times the initial P_ℓ concentration seems dramatic, but the resulting 0.8 µM P is still a very low concentration, normally considered highly growth limiting (Tinker and Nye, 2000). The root hairs increase plant P uptake most when placed where the P_ℓ increase is the greatest. The measured length of the hairs on the crown and lateral roots were not large enough to reach that zone (Table 2), but the hairs on the S-type laterals were placed across the rhizosphere.

The root and the sorbing soil pools competed for P in solution, as shown in the P balances in Figures 3c and 3d. Note that the uptake plotted in Figures 3a and 3b formed only a very small fraction of the total

P concentration in the crown- and L-type lateral rhizospheres. The pools of $P_{s,\text{slow}}$ (red line) and $P_{s,\text{fast-sol}}$ (purple line) were depleted at a much greater rate than the rate at which P was taken up because the pool of $P_{s,\text{fast}}$ (green line) adsorbed a large fraction of the released P. The movement between P fractions was largely driven by the pH change.

Crown roots achieved a greater pH change in the rhizosphere: at the root surface up to +1.05 pH units and at the outer boundary up to +0.76 units (Figures 4c and 4d). The greater pH change in the rhizosphere of crown roots was associated with their larger surface area (i. e. diameter and number of root hairs).

[Figure 4 about here]

3.4 | Sensitivity analysis

We analyzed the sensitivity of the P uptake to a relative change in the default parameters (Figures 5 and 6, note the log-log scale). Sensitive parameters have steep slopes and need to be determined accurately. They also present opportunities for increasing P uptake if the parameter values can be changed through breeding or agricultural management.

3.4.1 | Plant parameters

The radius r_1 is the radial distance to the mid-point between neighboring roots in the radial model. Reducing r_1 (which corresponds with an increase in RLD) increased the local pH change and the solubilization, especially in the case of crown roots. Hence, crown roots closer together take up more P. We excluded simulations with a change in pH of more than one unit as this would be outside the validity of the parameter ranges. Therefore, r_1 could be reduced by 40 % to approximately $r_1 = 0.2$ cm for the rhizosphere of L-type segments, obtaining ten times the initial P_ℓ locally (or here maximally by 45 % to $r_1 = 0.186$ cm with 17.5 times $P_{\ell,\text{init}}$). The sensitivity to r_1 thus demonstrates that intra-root facilitation increases with increasing RLD (Figure 5b).

Among the root parameters, morphological traits influence P uptake most (root hair length l_h, root hair

number N_h, root hair radius r_h, and S-type length L_{SR}, Figures 5a and 5b). Uptake by the root system was highly sensitive to root hair morphology (l_h, N_h, and r_h), with root hair length and number equally important (Figure 6). Uptake by L-type laterals was more sensitive than uptake by crown roots concerning change in root hair number, root hair radius, and S-type length (Figures 5b and 5a). The results suggest that there is more potential to increase the benefit of L-types. However, these sensitivity differences diminish at the whole root system level, because the contribution of uptake by L-type laterals to total uptake was less than that by thicker crown roots (see section 3.4.3).

Besides root morphology, the root-induced HCO_3^- efflux was very important in the model. The sensitivity to the efflux was in the range of the root morphological parameters for L-types (pink line in Figures 5a and 5b). Additional S-types in the rhizosphere were beneficial (brown line).

3.4.2 | Soil parameters

We recap that α denotes the fraction of NaOH-P_i, which dissolves when the pH increases, and β the ratio of the slow pools in steady-state at initial pH and unit pH increase. The parameters α and β are estimated, not measured. However, the simulated uptake was not sensitive to them (Figures 5c and 5d). Insensitivity to α means that the pools of $P_{s,\text{fast-sol}}$ and $P_{s,\text{slow}}$ can replace each other. For example, the extreme case $\alpha = 1$ (no slow sorption) could compensate for the lack of a slow pH-dependent sorption (Supporting Information, Figure S2).

For the variation in slow sorption, we varied the reaction half-times with and without unit pH change ($t_{1/2}$ and $t^*_{1/2}$ in Eqns 35 and 36). The uptake increased when the starting half-time ($t_{1/2}$) of the slow pool increased or when the end half-time ($t^*_{1/2}$) decreased. A smaller $t^*_{1/2}$ led to greater depletion of the slow pool. The accelerated release in response to increased pH (i. e. the discrepancy between $t_{1/2}$ and $t^*_{1/2}$) influenced uptake strongly. Hence, $t_{1/2}$ and $t^*_{1/2}$ should be determined carefully to obtain accurate predictions of uptake. For example, an accelerated slow pH-dependent desorption could compensate for the lack of rapid solubilization (Supporting Information, Figure S2). Decreasing $t^*_{1/2}$ to 1 d resulted in approximately 130 % of the reference uptake (while

$\alpha = 0$), and decreasing $t_{1/2}$ to 14 d with $t^*_{1/2} = 2$ d resulted in approximately 90 % of the reference uptake ($\alpha = 0$).

We found that the fast and slow sorbing P pools (i. e. $P_{s,\text{fast}}$ and $P_{s,\text{slow}}$) compete for the P in solution, and the extent of this competition depends on the relative rates of the fast and slow adsorption-desorption reactions. Therefore, we specified a relatively large pH-dependent desorption rate to overcome the competition of slow and fast P pools by depletion of the slow P pool.

3.4.3 | Whole root system uptake

The total P uptake by the root system was less sensitive to the lengths of S-types, L-types, and crown roots (L_{SR}, L_{L}, and L_{C}) than to the root hair morphology (Figure 6). While the root length increased, the released HCO_3^- per segment decreased, and thereby the uptake. Hence, the resulting sensitivity was less than the 1:1-line. The sensitivity of uptake to L_{C} was greater than that to L_{L} and about the same as to L_{SR} in the rhizospheres of both parent roots. Note that the change in L_{C}, and L_{L} implied change in total S-type length.

Changing the relative proportions of S-type to L-type to crown root (volume, surface area, or length) did not affect uptake strongly (Figure 6). Increasing the proportion of the length of S-type laterals (ω_{S}) relative to the other two root classes affected uptake the least and slightly negative (solid black line, condition: $\omega_{\text{S}} + \omega_{\text{L}} + \omega_{\text{C}} = 1$). Because an increase in S-type length at the cost of L-types (ω_{L}) and crown roots (ω_{C}) reduces the total surface area and volume of the whole root system. The direct effect of smaller surface area on P uptake is moderated by the effect on HCO_3^- efflux, which is increased since the total HCO_3^- release per plant is fixed. Usually, trade-offs for investment into root classes are presented on a metabolic equivalence basis, either in terms of carbon or P. We do not know these costs in our system, but we may compare root system compositions with varying S-type lengths at a fixed total root surface area (dashed black line in Figure 6) or volume (gray line). Note that keeping surface area or volume fixed, an increase in ω_{S} increases the total root length ($\omega_{\text{S}} + \omega_{\text{L}} + \omega_{\text{C}} \neq 1$). Also, we kept the RLD fixed by varying r_1. An increase in S-type proportion but fixed total root surface area or volume resulted in only slightly more P uptake. Hence, the investment between

S-types and thicker root classes seems balanced in DJ123.

[Figure 5 about here]

[Figure 6 about here]

4 | DISCUSSION

4.1 | The importance of solubilization and its interaction with root morphology

Conventional models of P uptake in which roots are treated as sinks for P, but not otherwise influencing the solubility of P in the soil, work reasonably well for soils with large P concentrations in the soil solution. But for strongly P-sorbing soils, such as highly weathered soils of the humid tropics and volcanic ash soils, such models tend to greatly underestimate uptake. Hence, the model without solubilization could only account for 41 % of the observed uptake (Figure 2b). The full model allows for solubilization of P and interactions between solubilization and root morphology. The full model successfully predicts the total P uptake by the P-efficient upland rice genotype DJ123 growing in a strongly sorbing soil using input parameter values measured independently.

As P is removed from the soil by root uptake, a zone of depletion develops around the root (Figure 4). The depletion zone is narrow because P diffusion in the soil is very slow due to the strong sorption. However, simultaneously the root releases HCO_3^- ions into the soil to balance higher anion than cation intake, and the reaction of HCO_3^- with the soil tends to increase the P concentration in solution. In our simulations, HCO_3^- diffused faster than P and, consequently, a zone developed in which the P concentration in solution rose above that in the soil bulk. Thus peaks in P concentration in solution formed at approximately 0.1 cm from the crown root and 0.06 cm from the L-type (Figures 4a and 4b). Phosphate, therefore, diffuses from the solubilization zone, albeit very slowly (Supporting Information, Figure S4). This is where the interaction with fine S-type lateral roots branching off the parent root becomes important because the laterals and their hairs

may intercept solubilized P that would otherwise not be available to the plant. The increase in P uptake due to solubilization is thereby reinforced.

4.2 | Root-induced pH changes

Efflux of HCO_3^- from the roots depends on the excess influx of anions over cations, which depends on the rate of increase in total plant biomass, the nutrient composition of the plant, the root-shoot ratio, and root surface area. That means, for a fixed root surface area, the total HCO_3^- release increases as the rate of plant growth increases (Figures 5a and 5b, pink lines). Hence, a genotype with better internal P use efficiency (greater growth rate per unit root surface) can have better P uptake efficiency due to an increased HCO_3^- efflux and P solubilization.

We estimated HCO_3^- efflux from the total biomass with a typical nutrient composition of rice and used a constant efflux per unit root surface area. Therefore, crown roots induced greater pH change than L-type laterals (Figure 4). For a given efflux, root-induced pH changes will be greater with more compact root systems. Hence, at greater root length density, the distance between neighboring roots is smaller, and therefore the HCO_3^- accumulates in a smaller volume of soil, resulting in greater solubilization and uptake. However, this effect will be offset if the uptake of other nutrients, and hence the HCO_3^- efflux, is impaired at the greater rooting density.

Soil factors also influence the pH change away from the roots but were not studied in detail. The initial soil pH, the CO_2 pressure in the soil air, and the soil pH buffer power (Eqn 2) will therefore also influence P solubilization and uptake to some extent.

4.3 | Root P uptake kinetics

We assigned values for the root P uptake parameters such that they did not limit uptake, and there was no minimum concentration below which uptake ceased. In reality, there must be some minimum concentration

for P uptake transporters to operate. Rice plants can reduce solution P concentrations to 16 nM (Mori et al., 2016), however, reliable minimum concentrations are rarely documented (Griffiths and York, 2020). If the P transporter activity limited uptake to some minimum concentration, additional solubilization would be required to account for the observed rates of P uptake. There is a need to measure genotypic variation in root uptake parameters in the sub-micro-molar range as it may explain (among other traits) why some genotypes have lower uptake per unit root length than more P-efficient genotypes.

4.4 | Contributions of different root classes to uptake

S-type laterals increase net P uptake dramatically because they are positioned inside the solubilization zones but outside the P depletion zones of L-types and crown roots. Although the S-types have a small diameter, their effective surface area for P uptake is greatly increased by their hairs. They are therefore efficient in intercepting P solubilized by their parent root. Over time, as the zone of pH-change and P solubilization around the parent root spreads further into the soil, the importance of S-types 'reaching out' increases. Treating S-type laterals independent of parent roots reduced their contribution to total P-uptake from 30 % to 11 % (Supplemental Material, Figure S3). Likewise, using a model that did not explicitly allow for solubilization, Gonzalez et al. (2021) found that S-types contributed little to total P uptake by the root system. Nonetheless, they showed that the low P cost of forming S-type laterals can be recovered by their P uptake within a day, much faster than other root types. With a model allowing for solubilization, this period would be even shorter. This facilitation of P uptake among the root classes suggests that there needs to be a balanced investment into the different root classes to optimize uptake.

Crown roots contribute less to the total root length than other root types but much to the total root surface area because of their larger diameter (Table 2). That large surface area furthermore allows more root hairs to grow per unit root length. This explains why crown root hairs contribute most to total plant P uptake. In addition to crown root uptake, their role as a parental root in enhancing P uptake of S-type laterals is larger than for parental L-type laterals due to the greater pH change and P solubilization they cause. We conclude

that crown roots have an important role in P uptake, and this may explain why genotypes with many crown roots have high performance under low P, despite crown roots being metabolically expensive (Wissuwa et al., 2020).

The total uptake of the whole root system was not sensitive to changes in the partitioning of S-type length (Figure 6, gray and brown line). This suggests that the P-efficient genotype DJ123 achieves a good balance among the root classes.

4.5 | Influence of root hair morphology on uptake

In the model, root hairs compete for P in the soil solution with the perpendicular root surface, and most of the P is taken up by hairs (Figure 3). Overall, the simulated uptake is strongly increased in response to increased root hair length, number, and diameter (Figures 5 and 6). Zygalakis et al. (2011) found – with a model allowing for root hairs but not solubilization or S-type laterals – that hair density had a much smaller effect on the uptake than length. This was because the hairs rapidly depleted P in the soil volume between them so that increasing the hair density had little effect. In our simulations, most hairs on S-type laterals are outside of the depletion zone of the parent root but within the zone where solubilization increases the P concentration in the soil solution. Therefore more densely spaced hairs had a similar impact to longer hairs.

Nestler and Wissuwa (2016) found that differences among upland rice genotypes were mostly due to the ability to increase hair length in response to P deficiency, and all the measured hair parameters showed consistent variation across root types. However, compared to the length of root hairs reported for other graminaceous species (Marzec et al., 2015; Itoh and Barber, 1983b; Hill et al., 2010), rice root hairs seem short and those on the parent roots do not reach as far as the peak of solubilized P concentration. Presumably, the P returns per unit P invested are greater for hairy S-types (length $\leq$1 cm) than for longer hairs alone.

While less important than root hair length and density, we found hair radius did influence uptake (Figures 5 and 6). We are not aware of any published data on variation in root hair diameter in rice, but two-fold variation can be seen in images by Kim et al. (2007). Data from arabidopsis showed variation among genotypes

exceeding variations within a given genotype (Parker et al., 2000), suggesting that variations in root hair diameter should be explored as a potential way to increase P uptake.

4.6 | Time dynamics of whole root system P uptake

The upscaled P uptake curve follows the exponential increase in measured P uptake quite nicely (Figure 2). Our simulations, however, overestimate the uptake during earlier time points and are below the measured average at the last time point. The shape of the P uptake curve for the whole root system is largely determined by the shape of the root growth curve with little influence of temporal uptake dynamics per unit root segment (Figures 3a and 3b). In upscaling, we account for the cumulative uptake by younger and older roots. Since the root system is a combination of older and younger roots at any time, the time dynamics of solubilization at the rhizosphere scale averages out at the whole root system scale. It proved, therefore, difficult to improve the fit of the whole root system P uptake curve by changing the model parameters. Possibly, root length was underestimated in the field experiment, where collecting whole root systems is challenging. Also, additional processes may have contributed in the field, such as an increase in the contribution of mycorrhizal fungi.

4.7 | Trade-offs and feedbacks at the whole plant level

At the whole plant level, there may be feedbacks that enhance growth under P-limited conditions causing small rhizosphere effects to have an increasing impact over time (Wissuwa, 2003). Greater P uptake is likely to increase growth and also the uptake of other nutrients resulting in increased HCO_3^- efflux, solubilization, and eventually P uptake. This positive feedback would benefit from greater internal P use efficiency. It would also benefit from an optimal investment into the different root classes and root hairs to capture the solubilized P. We concluded earlier that DJ123 seems balanced in this respect. However, the uptake of other nutrients, particularly nitrogen, also influences the relative investment into root classes. The best root system for capturing NO_3^- may have long crown roots exploiting the whole soil volume (Dathe et al., 2016). Such

a diffuse and deep root system is likely to be less effective for P uptake. But since P uptake depends on solubilization, NO_3^- uptake is also important. Therefore there may be trade-offs for optimizing root architecture and morphology. Further model studies are needed to explore this.

5 | CONCLUSIONS

Our mechanistic model successfully simulates P uptake by the P-efficient genotype DJ123 growing on strongly sorbing soil. The model allows the interchange of P between the soil solid and solution through fast and slow, pH-dependent reactions and for the P-solubilizing effect of root-induced pH changes. The modeled root system contains three root classes, all hairy: crown roots, L-type laterals, and S-type laterals. The simulated uptake is a result of an important interaction between solubilization and the morphology of the upland rice root system. In the absence of solubilization or S-type laterals, the model could not account for the measured uptake. P uptake is less sensitive to total root length and root class proportions. But S-types greatly enhance overall P uptake because they extend across the solubilization zone around the parent and beyond its P depletion zone. Hence, S-type laterals, longer root hairs, and greater root length density can improve uptake. However, these S-types are particularly beneficial in the solubilization zone. Solubilization over time is greater around thicker roots and when root length density is high. The greater surface area that comes with thicker roots increases the release of HCO_3^-, which relates to the plant nutrient composition and relative growth rates. Root hairs and S-types do not achieve strong solubilization themselves, but their P uptake is facilitated by the near presence of thicker roots, especially nodal roots. We thus found a pronounced facilitative interaction between very fine laterals and their thicker parent root and this needs to be considered in formulating target traits for selecting P-efficient rice cultivars.

ACKNOWLEDGEMENTS

We thank Drs Naoki Moritsuka and Tovo Rakotoson for their help with the soil measurements.

DATA AVAILABILITY

Contact the corresponding author for experimental data or source code.

CONFLICT OF INTEREST

The authors declare that they have no competing interests.

AUTHOR'S CONTRIBUTIONS

The root data and model challenge was presented by MW. The model was developed by CK, GK, and JP. Code by CK. GK provided soil data, MW the plant data. Figures made by CK. CK wrote the manuscript with input from all authors. All authors approved the final version of the manuscript.

REFERENCES

Alewell, C., Ringeval, B., Ballabio, C., Robinson, D. A., Panagos, P. and Borrelli, P. (2020) Global phosphorus shortage will be aggravated by soil erosion. *Nature Communications*, **11**, 4546.

Baldwin, J. P., Nye, P. H. and Tinker, P. B. (1973) Uptake of solutes by multiple root systems from soil. *Plant and Soil*, **38**, 621–635.

Barrow, N. J. (2008) The description of sorption curves. *European Journal of Soil Science*, **59**, 900–910.

— (2017) The effects of pH on phosphate uptake from the soil. *Plant and Soil*, **410**, 401–410.

Bhat, K. K. S., Nye, P. H. and Baldwin, J. P. (1976) Diffusion of phosphate to plant roots in soil. IV. the concentration distance profile in the rhizosphere of roots with root hairs in a low-P soil. *Plant and Soil*, **44**, 63–72.

Darmovzalova, J., Boghi, A., Otten, W., Eades, L. J., Roose, T. and Kirk, G. J. D. (2020) Uranium diffusion and time-dependent adsorption–desorption in soil: A model and experimental testing of the model. *European Journal of Soil Science*, **71**, 215–225.

Dathe, A., Postma, J. A., Postma-Blaauw, M. B. and Lynch, J. P. (2016) Impact of axial root growth angles on nitrogen acquisition in maize depends on environmental conditions. *Annals of Botany*, **118**, 401–414.

De Bauw, P., Mai, T. H., Schnepf, A., Merckx, R., Smolders, E. and Vanderborght, J. (2020) A functional–structural model of upland rice root systems reveals the importance of laterals and growing root tips for phosphate uptake from wet and dry soils. *Annals of Botany*, **126**, 789–806.

Dijkshoorn, W., Lathwell, D. J. and De Wit, C. T. (1968) Temporal changes in carboxylate content of ryegrass with stepwise change in nutrition. *Plant and Soil*, **29**, 369–390.

Dobermann, A. and Fairhurst, T. (2000) *Rice: Nutrient Disorders & Nutrient Management.* International Rice Research Institute.

Gamuyao, R., Chin, J. H., Pariasca-Tanaka, J., Pesaresi, P., Catausan, S., Dalid, C., Slamet-Loedin, I., Tecson-Mendoza, E. M., Wissuwa, M. and Heuer, S. (2012) The protein kinase Pstol1 from traditional rice confers tolerance of phosphorus deficiency. *Nature*, **488**, 535–539.

Gonzalez, D., Postma, J. A. and Wissuwa, M. (2021) Cost-benefit analysis of the upland-rice root architecture in relation to phosphate: 3D Simulations highlight the importance of S-type lateral roots for reducing the pay-off time. *Frontiers in Plant Science*, **12**, 359.

Griffiths, M. and York, L. M. (2020) Targeting Root Ion Uptake Kinetics to Increase Plant Productivity and Nutrient Use Efficiency. *Plant Physiology*, **182**, 1854–1868.

Hedley, M. J., Kirk, G. J. R. and Santos, M. B. (1994) Phosphorus efficiency and the forms of soil phosphorus utilized by upland rice cultivars. *Plant and Soil*, **158**, 53–62.

Hedley, M. J., White, R. E. and Nye, P. H. (1982) Plant-induced changes in the rhizosphere of rape (Brassica Napus Var. Emerald) seedlings. *New Phytologist*, **91**, 45–56.

Hill, J. O., Simpson, R. J., Ryan, M. H., Chapman, D. F., Hill, J. O., Simpson, R. J., Ryan, M. H. and Chapman, D. F. (2010) Root hair morphology and mycorrhizal colonisation of pasture species in response to phosphorus and nitrogen nutrition. *Crop and Pasture Science*, **61**, 122–131.

Hinsinger, P., Brauman, A., Devau, N., Gérard, F., Jourdan, C., Laclau, J.-P., Le Cadre, E., Jaillard, B. and Plassard, C. (2011) Acquisition of phosphorus and other poorly mobile nutrients by roots. Where do plant nutrition models fail? *Plant and Soil*, **348**, 29–61.

Hoffland, E. (1992) Quantitative evaluation of the role of organic acid exudation in the mobilization of rock phosphate by rape. *Plant and Soil*, **140**, 279–289.

Itoh, S. and Barber, S. A. (1983a) A numerical solution of whole plant nutrient uptake for soil-root systems with root hairs. *Plant and Soil*, **70**, 403–413.

— (1983b) Phosphorus Uptake by Six Plant Species as Related to Root Hairs1. *Agronomy Journal*, **75**, 457–461.

Kant, J., Ishizaki, T., Pariasca-Tanaka, J., Rose, T., Wissuwa, M. and Watt, M. (2018) *Phosphorus Efficient Phenotype of Rice*, 129–148. IntechOpen.

Kim, C. M., Park, S. H., Je, B. I., Park, S. H., Park, S. J., Piao, H. L., Eun, M. Y., Dolan, L. and Han, C.-d. (2007) Oscsld1, a cellulose synthase-like D1 gene, is required for root hair morphogenesis in rice. *Plant Physiology*, **143**, 1220–1230.

Kirk, G. J. D. (1999) A model of phosphate solubilization by organic anion excretion from plant roots. *European Journal of Soil Science*, **50**, 369–378.

Kirk, G. J. D., Santos, E. E. and Santos, M. B. (1999) Phosphate solubilization by organic anion excretion from rice growing in aerobic soil: rates of excretion and decomposition, effects on rhizosphere pH and effects on phosphate solubility and uptake. *New Phytologist*, **142**, 185–200.

Kuppe, C. W., Huber, G. and Postma, J. A. (2021a) Comparison of numerical methods for radial solute transport to simulate uptake by plant roots. *Rhizosphere*, 100352.

Kuppe, C. W., Schnepf, A., von Lieres, E., Watt, M. and Postma, J. A. (2021b) Rhizosphere models: their concepts and application to plant-soil ecosystems. *Plant and Soil*.

Leitner, D., Klepsch, S., Ptashnyk, M., Marchant, A., Kirk, G. J. D., Schnepf, A. and Roose, T. (2010) A dynamic model of nutrient uptake by root hairs. *New Phytologist*, **185**, 792–802.

Marzec, M., Melzer, M. and Szarejko, I. (2015) Root Hair Development in the Grasses: What We Already Know and What We Still Need to Know. *Plant Physiology*, **168**, 407–414.

Mori, A., Fukuda, T., Vejchasarn, P., Nestler, J., Pariasca-Tanaka, J. and Wissuwa, M. (2016) The role of root size versus root efficiency in phosphorus acquisition in rice. *Journal of Experimental Botany*, **67**, 1179–1189.

Murphy, J. and Riley, J. (1962) A modified single solution method for the determination of phosphate in natural waters. *Analytica Chimica Acta*, **27**, 31–36.

Nardi, P., Akutsu, M., Pariasca-Tanaka, J. and Wissuwa, M. (2013) Effect of methyl 3-4-hydroxyphenyl propionate, a sorghum root exudate, on N dynamic, potential nitrification activity and abundance of ammonia-oxidizing bacteria and archaea. *Plant Soil*, **367**, 627–637.

Nestler, J., Keyes, S. D. and Wissuwa, M. (2016) Root hair formation in rice (*Oryza sativa L.*) differs between root types and is altered in artificial growth conditions. *Journal of Experimental Botany*, **67**, 3699–3708.

Nestler, J. and Wissuwa, M. (2016) Superior root hair formation confers root efficiency in some, but not all, rice genotypes upon P deficiency. *Frontiers in Plant Science*, **7**, 1935.

Nye, P. H. (1981) Changes of pH across the rhizosphere induced by roots. *Plant and Soil*, **61**, 7–26.

— (1983) The diffusion of two interacting solutes in soil. *Journal of Soil Science*, **34**, 677–691.

Oburger, E., Kirk, G. J., Wenzel, W. W., Puschenreiter, M. and Jones, D. L. (2009) Interactive effects of organic acids in the rhizosphere. *Soil Biology and Biochemistry*, **41**, 449–457.

Parker, J. S., Cavell, A. C., Dolan, L., Roberts, K. and Grierson, C. S. (2000) Genetic interactions during root hair morphogenesis in arabidopsis. *The Plant Cell*, **12**, 1961–1974.

Penn, C. J. and Camberato, J. J. (2019) A critical review on soil chemical processes that control how soil pH affects phosphorus availability to plants. *Agriculture*, **9**.

Rakotoson, T., Holz, M. and Wissuwa, M. (2020) Phosphorus deficiency tolerance in *Oryza sativa*: Root and rhizosphere traits. *Rhizosphere*, **14**, 100198.

Rose, T. J., Impa, S. M., Rose, M. T., Pariasca-Tanaka, J., Mori, A., Heuer, S., Johnson-Beebout, S. E. and Wissuwa, M. (2013) Enhancing phosphorus and zinc acquisition efficiency in rice: A critical review of root traits and their potential utility in rice breeding. *Annals of Botany*, **112**, 331–345.

Schatz, M. C., Maron, L. G., Stein, J. C., Wences, A. H., Gurtowski, J., Biggers, E., Lee, H., Kramer, M., Antoniou, E., Ghiban, E., Wright, M. H., Chia, J.-m., Ware, D., McCouch, S. R. and McCombie, W. R. (2014) Whole genome de novo assemblies of three divergent strains of rice, Oryza sativa , document novel gene space of aus and indica. *Genome Biology*, **15**, 1–16.

Shampine, L. F. and Reichelt, M. W. (1997) The MATLAB ODE Suite. *SIAM Journal on Scientific Computing*, **18**, 1–22.

Tinker, P. and Nye, P. (2000) *Solute Movement in the Rhizosphere*. Topics in Sustainable Agronomy. Oxford University Press.

Vandamme, E., Rose, T., Saito, K., Jeong, K. and Wissuwa, M. (2016) Integration of P acquisition efficiency, P utilization efficiency and low grain P concentrations into P-efficient rice genotypes for specific target environments. *Nutrient Cycling in Agroecosystems*, **104**, 413–427.

Wissuwa, M. (2003) How do plants achieve tolerance to phosphorus deficiency? small causes with big effects. *Plant Physiology*, **133**, 1947–1958.

— (2005) Combining a modelling with a genetic approach in establishing associations between genetic and physiological effects in relation to phosphorus uptake. *Plant and Soil*, **269**, 57–68.

Wissuwa, M., Gonzalez, D. and Watts-Williams, S. J. (2020) The contribution of plant traits and soil microbes to phosphorus uptake from low-phosphorus soil in upland rice varieties. *Plant and Soil*, **448**, 523–537.

Wissuwa, M., Kondo, K., Fukuda, T., Mori, A., Rose, M. T., Pariasca-Tanaka, J., Kretzschmar, T., Haefele, S. M. and Rose, T. J. (2015) Unmasking novel loci for internal phosphorus utilization efficiency in rice germplasm through genome-wide association analysis. *PLOS ONE*, **10**, 1–21.

706 Yamauchi, A., Kono, Y. and Tatsumi, J. (1987) Comparison of root system structures of 13 species of cereals.
707 *Japanese journal of crop science*, **56**, 618–631.

708 Zygalakis, K. C., Kirk, G. J. D., Jones, D. L., Wissuwa, M. and Roose, T. (2011) A dual porosity model of nutrient
709 uptake by root hairs. *New Phytologist*, **192**, 676–688.

TABLE 1 List of main symbols

Symbol	Definition	Unit
P	concentration of P in the whole soil	mol cm^{-3} (soil)
P_ℓ	concentration of P in soil solution	mol cm^{-3} (solution)
$P_{s,\text{fast}}$	concentration of P in rapid equilibrium with the soil solution at the initial pH	mol g^{-1} (soil)
$P_{s,\text{fast-sol}}$	concentration of P rapidly solubilized as the pH is increased	mol g^{-1} (soil)
$P_{s,\text{slow}}$	concentration of P in slow equilibrium with the solution	mol g^{-1} (soil)
B_ℓ	concentration of HCO_3^- in soil solution	mol cm^{-3} (solution)
H_ℓ	concentration of H_3O^+ in soil solution	mol cm^{-3} (solution)
b_P	soil buffer power at initial B_ℓ, defined as $\theta + \rho\left(\partial P_{s,\text{fast}}/\partial P_\ell\right)_{B_\ell}$	cm^3 (solution) cm^{-3} (soil)
b_HS	soil pH buffer power, defined as $-\partial HS/\partial\text{pH}$ where HS is the concentration of titratable acidity in the soil	mol cm^{-3} (soil) (pH unit)$^{-1}$
λ	soil P-HCO_3^- interaction coefficient, defined as $\left(\partial P_\ell/\partial B_\ell\right)_P$	
D_H, D_B, D_P	diffusion coefficient in free solution for H_3O^+, HCO_3^-, and $H_2PO_4^-$, respectively	cm^2 s^{-1}
θ	soil volumetric water content	cm^3 (solution) cm^{-3} (soil)
ρ	soil bulk density	g cm^{-3} (soil)
f	diffusion impedance factor	
r_0	root radius	cm
r_1	outer radius (from root center)	cm
I_R	uptake rate inside the rhizosphere including root hairs I_h, S-type laterals I_S, and S-type hairs I_hS	mol cm^{-3} (soil) s^{-1}
E_R	efflux into the rhizosphere including root hairs E_h, S-type laterals E_S, and S-type hairs E_hS	mol cm^{-3} (soil) s^{-1}
E	efflux of base HCO_3^-	mol cm^{-2} (root) s^{-1}
t	time dimension	d
r	space dimension (symmetrical radial coordinates)	cm

TABLE 2 S-type, L-type, and crown root default parameters of rice genotype DJ123

Parameter		S-type	L-type	crown roots	Unit	Source
Root radius	r_0	$r_S = 0.0025$	0.01	0.03	cm	WinRhizo and ImageJ plus Micrograph
Outer radius	r_1	$r_{h1_{S,surf}}$	0.3386	0.3386	cm	outer boundary derived from RLD, Eqn 26
Number of root hairs per unit segment on: $2r_0\pi$L, L = 1 cm	N_h	$N_{hS} = 520$ (420−620)[a]	700 (600−825)[a]	1440 (1360−1520)[a]	cm^{-1}	Nestler and Wissuwa (2016)
Root hair length	l_h	$l_{hS} = 0.0125$ (0.01−0.0155)[a]	0.014 (0.012−0.017)[a]	0.02 (0.017−0.0225)[a]	cm	Nestler and Wissuwa (2016)
Root hair radius	r_h	0.0008	0.0008	0.0008	cm	Nestler et al. (2016), diameter 10–20 µm
Length proportion[b]	ω	0.5	0.33	0.17	fraction	Wissuwa et al. (2020)
Surface area proportion		0.21	0.31	0.48	fraction	(including hairs)

a) Values in brackets are 'field' to 'box' data, we used a value within that range. b) here a 3:2:1-ratio as default.

TABLE 3 Soil P fractions measured in the experimental soil measured by the Hedley et al. (1982) sequential fractionation scheme

Extraction step	Fraction	Content
		(mmol kg^{-1})
1 g soil with 26 μmol HCO_3^--form anion exchange resin in H_2O, recovering P from the resin in 0.5 M HCl	Resin-P	0.04
30 cm^3 of 0.5 M $NaHCO_3$, followed by digestion of the extract in H_2SO_4 and H_2O_2	$NaHCO_3$-P_i	0.46
P_o inferred from total P less P_i	$NaHCO_3$-P_o	0.71
30 cm^3 of 0.1 M NaOH, followed by digestion of the extract in H_2SO_4 and H_2O_2	NaOH-P_i	11.29
P_o inferred from total P less P_i	NaOH-P_o	5.72
30 cm^3 of 1 M HCl	HCl-P	0.74
digestion of the residual soil in H_2SO_4 and H_2O_2	Residual-P	21.06
	Total	40.02

P_i: inorganic, P_o: organic

TABLE 4 Parameters and intermediates for default simulation.

Parameter	Value	Unit	Comments
V_{max}	8×10^{-12}	mol cm^{-2} s^{-1}	maximal P uptake rate (assumed to be fast)
K_m	1×10^{-9}	mol cm^{-3}	concentration at which P uptake rate is $\frac{1}{2}V_{max}$ (assumed to be low)
ρ	0.87	g cm^{-3}	bulk density for Andosol
θ	0.3	cm^3 cm^{-3}	volumetric water content
f	0.24		diffusion impedance factor for Andosol
D_P	8.9×10^{-6}	cm^2 s^{-1}	$H_2PO_4^-$ diffusion coefficient in water
D_B	1.23×10^{-5}	cm^2 s^{-1}	HCO_3^- diffusion coefficient in water
D_H	9.55×10^{-5}	cm^2 s^{-1}	H_3O^+ diffusion coefficient in water
K_1	4.45×10^{-10}	mol cm^{-3}	apparent first dissociation constant of H_2CO_3
K_s	3.39×10^{-5}	mol cm^{-3} atm^{-1}	solubility of CO_2 in water
p_{CO_2}	4×10^{-3}	atm	CO_2 pressure in soil air
α	0.33		fraction of [NaOH-P_i] to calculate λ
β	0.4		relative change in $P_{s,slow}(t = 0)$ in steady-state after pH change
λ	1.49×10^{-3}		soil P_ℓ-B_ℓ interaction coefficient, dP_ℓ/dB_ℓ at constant P_ℓ
$t_{1/2}$	28	d	half-time of slow sorption reaction at pH of 5.8
$t^*_{1/2}$	2	d	half-time of slow sorption reaction at pH of 6.861
k_1	7.86×10^{-2}	s^{-1}	reaction constant in Eqn 13
k_2	2.87×10^{-7}	s^{-1}	reaction constant in Eqn 14, half-time of 28 d
k^*_1	1.34×10^5	cm^3 mol^{-1} s^{-1}	reaction constant in Eqn 13
k^*_2	9.31	cm^3 mol^{-1} s^{-1}	reaction constant in Eqn 14
b_P	5440		soil buffer power of P, $b_P = \theta + \rho P_{s,fast}/P_\ell$, at $t = 0$
b_{HS}	1×10^{-5}	mol cm^{-3} (pH unit)$^{-1}$	pH buffer capacity
E	1.83×10^{-12}	mol cm^{-2} s^{-1}	efflux flux of HCO_3^- across root surface
$P_{\ell,init}$	8×10^{-11}	mol cm^{-3}	initial P in solution
$pH_{initial}$	5.8		initial pH (1:5 H_2O) measured for Andosol
ΔB_ℓ	4×10^{-7}	mol cm^{-3}	see Eqn 34

parameters per second are converted to days for the time dimension t.

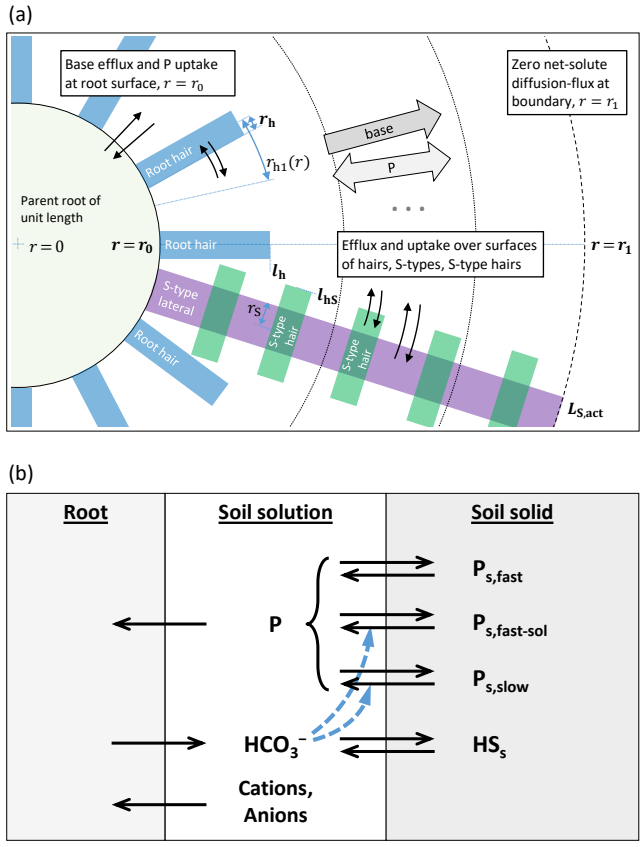

FIGURE 1 (a) The geometry of the model showing the S-type lateral and the root hairs associated with the parent root (crown or L-type lateral roots); (b) The interchange of P between the soil solid and solution, represented as fast and slow reactions, both sensitive to the concentration of soil bases (HCO_3^-); the symbols are defined in Tables 1 and 2.

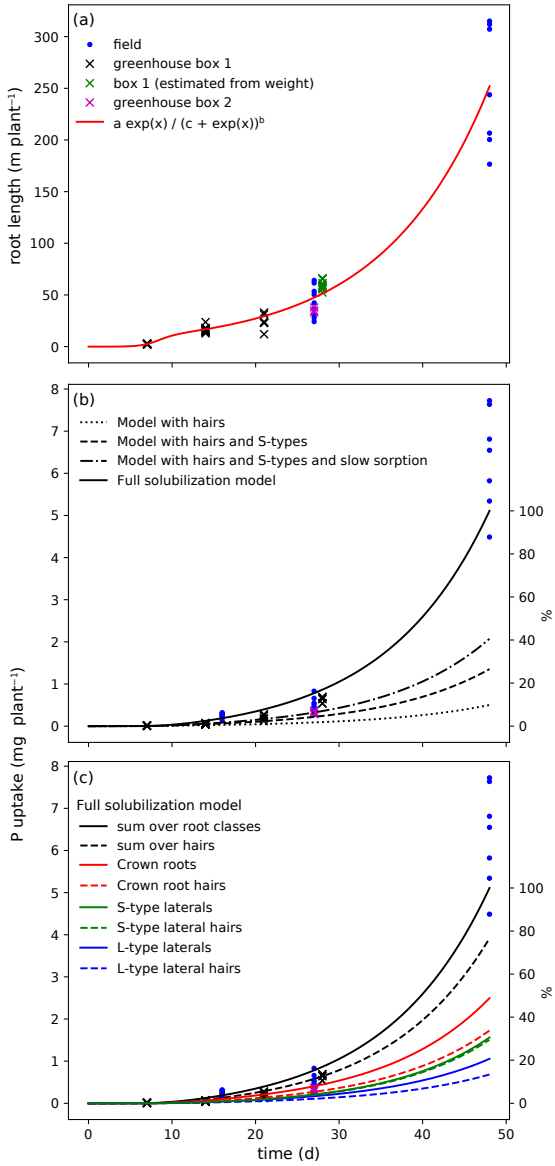

FIGURE 2 (a) Measured time course of root system length (points) and the fitted function $L(t) = a\exp(t)/(c + \exp(t))^b$ with parameters $a = 555$, $b = 0.92$, $c = 3627$ ($R^2 = 0.928$). (b) Simulated P uptake with (solid line) or without (dashed lines) solubilization, and with and without S-type laterals (21% less surface area) and slow P desorption. (c) Simulated contributions of individual root classes including their root hairs (solid lines) and their hairs only (dashed lines) to P uptake.

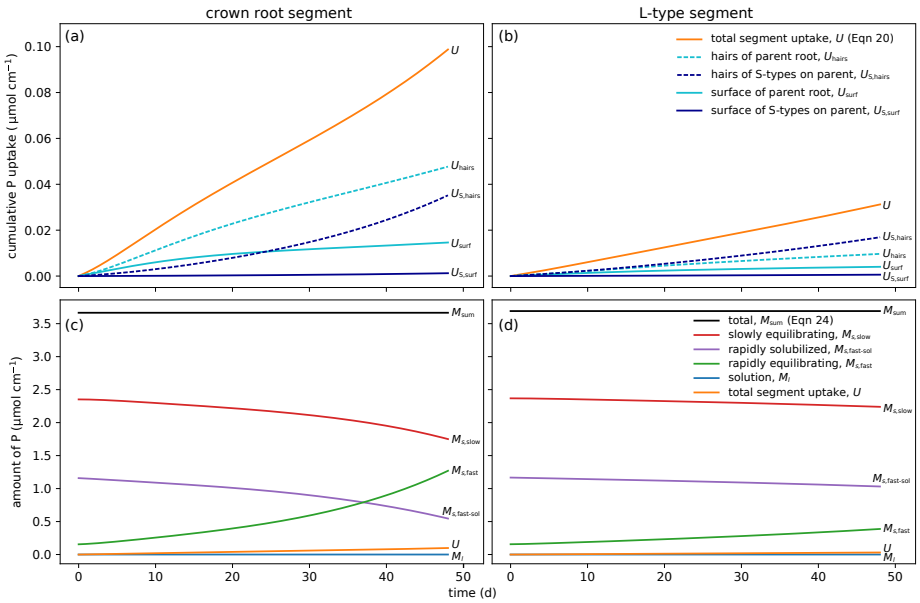

FIGURE 3 (a), (b) Cumulative P uptake by the surface and hairs of crown roots and L-type laterals of unit length, respectively; and (c), (d) the amount of P in the rhizosphere-volume of crown roots and L-type laterals, respectively.

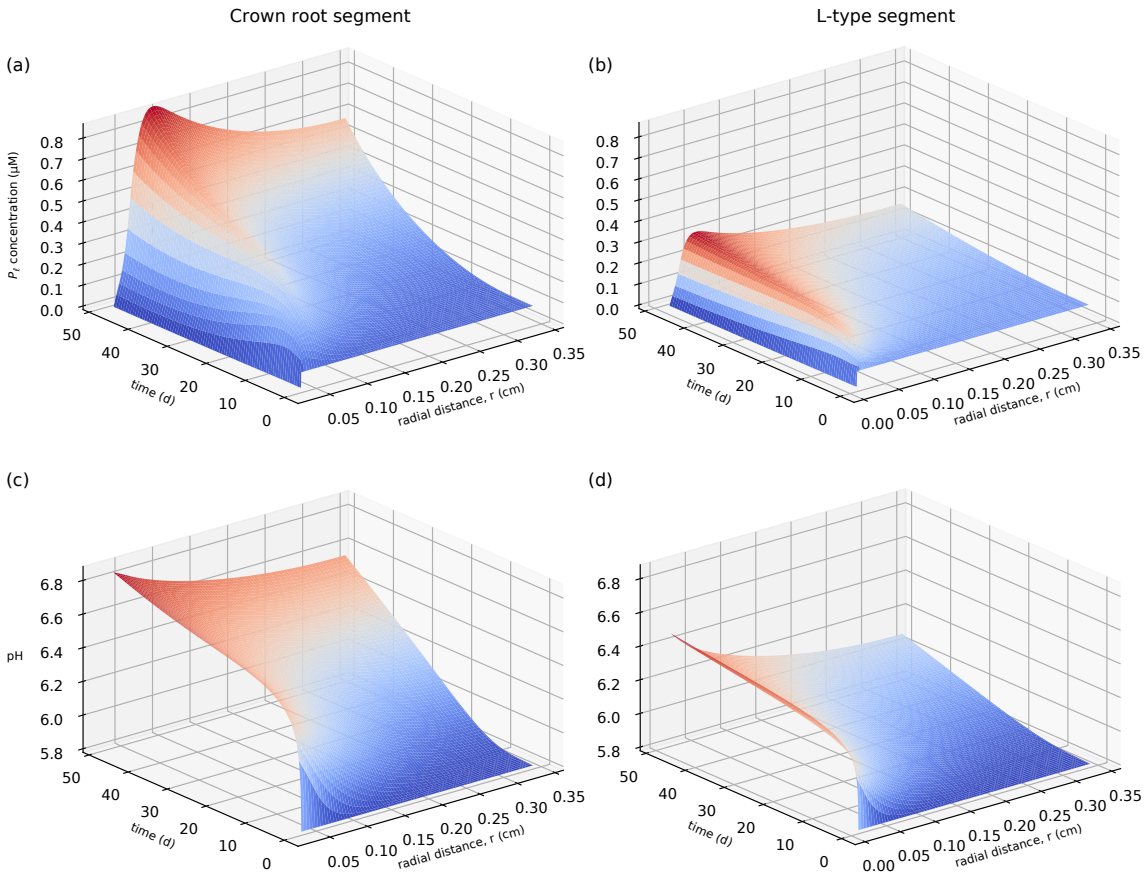

FIGURE 4 Concentration profiles over time and radial distance of (a), (b) P in the soil solution and (c), (d) pH for crown roots and L-type laterals. The model parameter values have the standard values given in Tables 2 and 4. Note that the center of the segment is located at $r = 0$ and the root surface at $r = r_0$. Colors follow the contour lines.

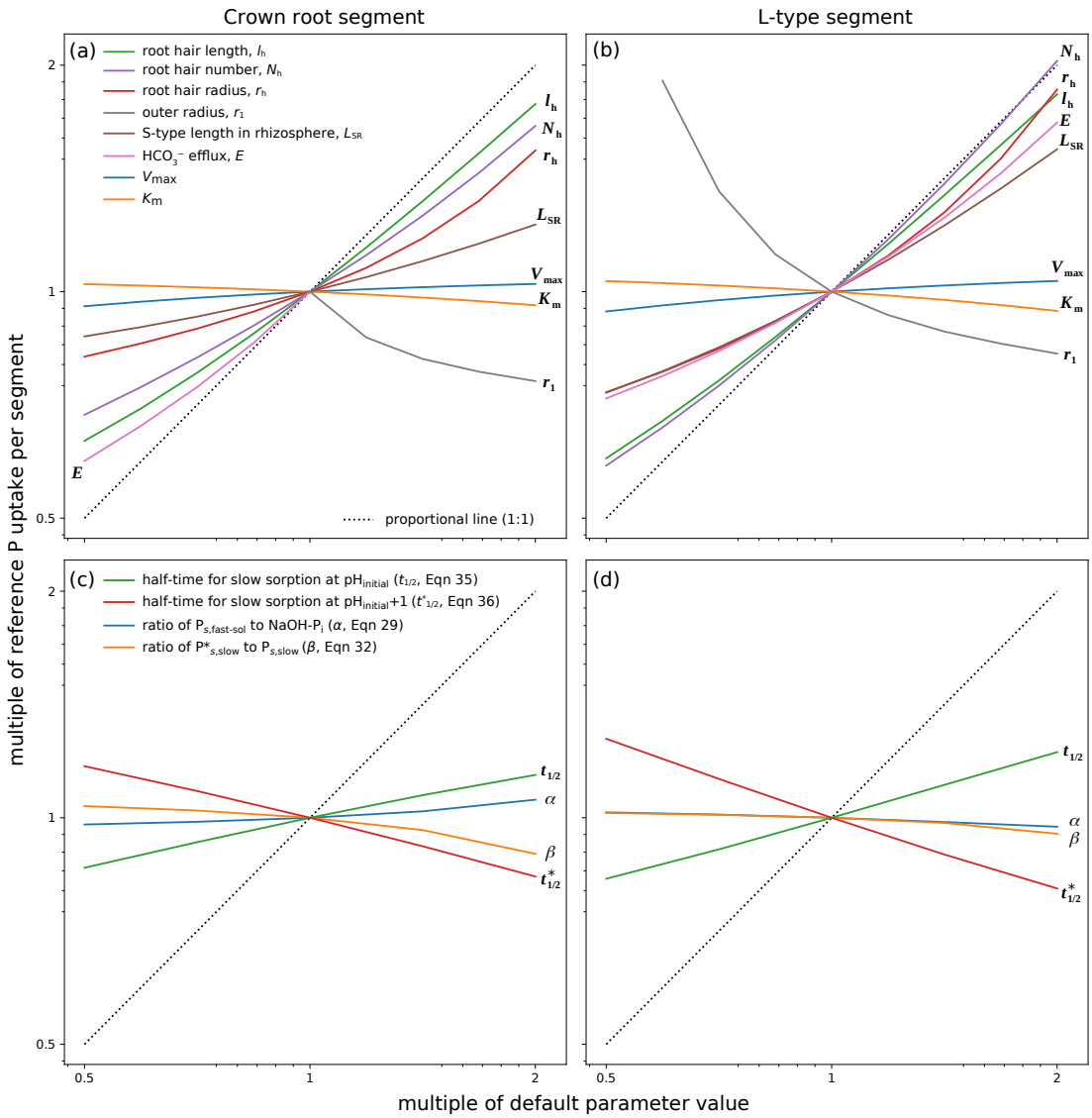

FIGURE 5 Sensitivity of P uptake per unit root length to model input parameters as multiples of the standard values: (a) and (b) root parameters; (c) and (d) soil parameters. The total release of HCO_3^- per plant is fixed as the root parameters vary (i. e. for surface area variations), and the total amount of P in soil is kept constant as the soil parameters vary. The parameters r_1 and efflux are varied in a range without changing the pH locally by more than one unit (pink line and grey line). Note axes are logarithmic.

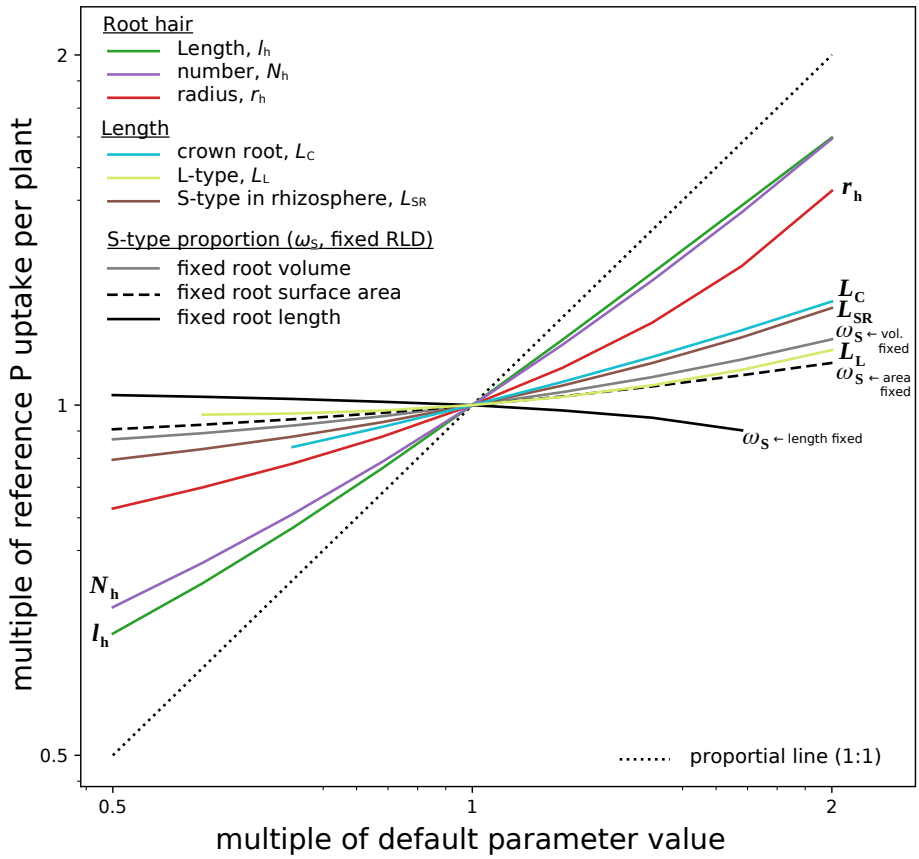

FIGURE 6 Sensitivity of total P uptake by the root system to model input parameters as multiples of the standard values. Note axes are logarithmic.

Supporting Information: Phosphate solubilization and uptake by upland rice in strongly sorbing soil

Derivation of the P-pH coupling

We derive the (rapid) solubilization of in Eqn 6 via the total differential (see Eqn 2 in Nye, 1983),

$$\Delta P_\ell = \frac{\partial P_\ell}{\partial P_\mathrm{e}} \Delta P_\mathrm{e} + \frac{\partial P_\ell}{\partial B_\ell} \Delta B_\ell \tag{S1}$$

with $P_\mathrm{e} = \theta P_\ell + \rho \left(P_{s,\mathrm{fast}} + P_{s,\mathrm{fast\text{-}sol}} \right)$. Both gradients are constants, hence, substitution of $b_\mathrm{P} = \partial P_\mathrm{e} / \partial P_\ell$ and $\lambda = \partial P_\ell / \partial B_\ell$, and rearranging gives

$$\Delta P_\mathrm{e} = b_\mathrm{P} \Delta P_\ell - \lambda b_\mathrm{P} \Delta B_\ell \tag{S2}$$

which is infinitesimally

$$\frac{d P_\mathrm{e}}{dt} = b_\mathrm{P} \left(\frac{d P_\ell}{dt} - \lambda \frac{d B_\ell}{dt} \right). \tag{S3}$$

Adding $g = \rho \partial P_{s,\mathrm{slow}} / \partial t$ gives Eqn 6 with left-hand-side as in Eqn 5. Here, P_ℓ does not influence $P_{s,\mathrm{fast\text{-}sol}}$ ($\partial P_{s,\mathrm{fast\text{-}sol}} / \partial P_\ell = 0$ and $b_\mathrm{P} \partial P_\ell / \partial t = \theta \partial P_\ell / \partial t + \rho \partial P_{s,\mathrm{fast}} / \partial t$), but the pH change from an initial pH determines the relevant total P concentration. In our simulation, the solubilization of solid phase P is a source according to Eqn 33, i. e. the initial concentration of $P_{s,\mathrm{fast\text{-}sol}}$ decreases (Eqn 29). Due to the release of HCO_3^- by the root, we have $\partial B_\ell / \partial t > 0$ and $\partial P_{s,\mathrm{fast\text{-}sol}} / \partial t < 0$. In general, the coupling gradient $\partial B_\ell / \partial t$ could change sign, and when negative (pH declines), the P_ℓ concentration would move to the solid phase.

Parameterization of the pH coupling in the model

For other pH ranges, the model can be adapted by sign-change of λ to perform in the opposite direction of pH change, i. e. pH decrease (increase) resulting in increase (decrease) of available P concentration. Note that a sign-change of λ implies a sign-change of ΔP_e or ΔB_ℓ^* in Eqn 33, respectively, such that $\Delta P_\ell = 0$.

Uptake and efflux by S-type laterals

The S-type lateral roots were treated as part of the sink term in Eqn 8 analog to Eqn 15 for hairs of parent root. This resulted in additional surface per volume for the S-types branching of the 1 cm root segment, $A_{\mathrm{S,surf}}$, and S-type root hair surface area, $A_{\mathrm{S,hairs}}$ in the rhizosphere, r_0 to r_1. The P uptake rates by S-types and their hairs are

$$I_\mathrm{S} = V \left(r_\mathrm{S}, r_{\mathrm{h1}_{\mathrm{S,surf}}} \right) A_{\mathrm{S,surf}}, \tag{S4}$$

and

$$I_\mathrm{hS} = V \left(r_\mathrm{h}, r_{\mathrm{h1}_{\mathrm{S,hairs}}} \right) A_{\mathrm{S,hairs}}, \tag{S5}$$

where the influx function $V = V_{\max} P_{\mathrm{rh}}/(K_{\mathrm{m}} + P_{\mathrm{rh}})$ is evaluated with corresponding $P_{\mathrm{rh}}(P_{\ell}, r_{\mathrm{S}}, r_{\mathrm{h1}_{\mathrm{S,surf}}})$ and $P_{\mathrm{rh}}(P_{\ell}, r_{\mathrm{h}}, r_{\mathrm{h1}_{\mathrm{S,hairs}}})$ for the radii of S-type, r_{S}, and S-type hair, r_{h}; the mid-distances to neighboring S-type branches, $r_{\mathrm{h1}_{\mathrm{S,surf}}} = \sqrt{r\pi/\left(2N_{\mathrm{Scm}}\right)}$, and S-type root hairs, $r_{\mathrm{h1}_{\mathrm{S,hairs}}} = \sqrt{r_{\mathrm{S}}\pi/\left(2N_{\mathrm{hS}}\right)}$; and the solution concentration $P_{\ell}(r,t)$, respectively, see Eqn 18 and Eqn 15.

The continuous description of surface area per rhizosphere volume for the S-type segment with an infinitesimal parameter, δ, is

$$A_{\mathrm{S,surf}} = \frac{2r_{\mathrm{S}} N_{\mathrm{Scm}} \delta}{(r+\delta)^2 - r^2} \tag{S6}$$

where r_{S} is the S-type radius and $N_{\mathrm{Scm}} = L_{\mathrm{SR}}/L_{\mathrm{S,act}}$ is the number of S-types per cm root. The surface area per rhizosphere volume for S-type root hairs is

$$A_{\mathrm{S,hairs}} = \frac{2r_{\mathrm{h}} l_{\mathrm{hS}} N_{\mathrm{Scm}} N_{\mathrm{hS}} \delta}{(r+\delta)^2 - r^2} \tag{S7}$$

where l_{hS} is the length of an S-type root hair, r_{h} the root hair radius, and N_{hS} the number of root hairs on 1 cm S-type (Table 2).

Upscaling over root classes

$$\mathcal{P}(t) = \sum_{i \in M} \mathcal{P}_i(t) = \int_0^t \sum_{i \in M} \omega_i \dot{L}(s) U_i(t-s) \mathrm{d}s, \tag{S8}$$

where $M := \{\mathrm{L}, \mathrm{C}\}$, and length-partition weight, ω_i (Table 2). Discretized, we derive the upscaled P uptake for each root class at t_j by

$$\mathcal{P}_i(t_j) = \omega_i \sum_{k=1}^{j} \Delta L_k \, U_i(t_{j+1-k}), \tag{S9}$$

where $U_i(t_*)$ is the cumulative uptake up to time point t_* for root class i. The difference $\Delta L_k = L(t_k) - L(t_{k-1})$ is the length that is added to the total root system length at t_k.

Model implementation

In the time-direction, the system was solved using BDF (backward differentiation formula as described in Shampine and Reichelt, 1997), an implicit variable-order (1–5) method with quasi-constant step size. We used Pythons Scipy implementation of the BDF, a relative error tolerance of 1×10^{-5}. The initial time step was 1×10^{-10} d. We iterated over the line-discretizations of the right-hand-side of the differential equations for HCO_3^-, P_{ℓ}, and $P_{s,\mathrm{slow}}$ in one time-sweep. In this system, hence with BDF and the same stepping, we also integrated: the uptake for the root hairs, the root surface, and S-type (hairs and surface separately) of the parent.

The spatial discretization of the diffusive transport was of second-order (central difference for second derivatives, cubic upwind interpolation for the first derivatives). Main root hairs and S-type surface area per volume were spatially discretized as in Kuppe et al. (2021a). We used a spatial step size of $\Delta r = 1.2344 \times 10^{-3}$ cm for crown roots and $\Delta r = 1.3144 \times 10^{-3}$ cm for L-types.

Supplemental Figures

S1 We calculated the amount of HCO_3^- per plant based on the plant biomass, which is supposed to correlate with nitrate uptake where the roots release HCO_3^-.

S2 We calculated and compared several parameter combinations, showing that the measured P uptake can be simulated with parameters that are far away from the measured ones.

S3 When not combining S-type laterals to the parent root rhizosphere but simulating them as separate root class with the parameters from table 4, we did not achieve the measured P uptake, and the relative importance of L-types and S-types change places in their ranking.

S4 In strongly sorbing soil, the P in solution diffuses slowly.

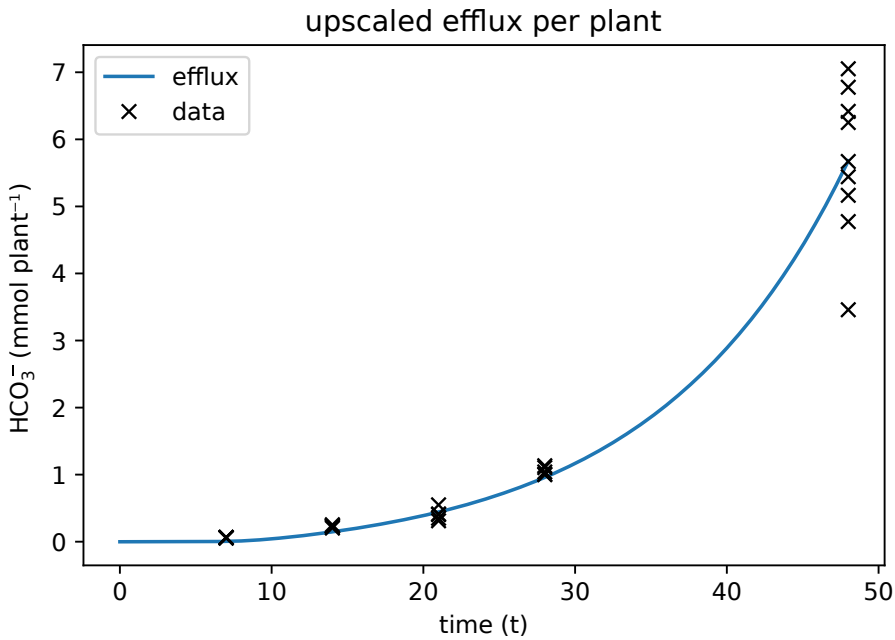

FIGURE S1 Amount of released HCO_3^- of the total root system, integrated (upscaled) and derived from data. This curve was fixed for the sensitivity analysis of the plant traits. Data is based on total dry weight scaled by 1.49 mmol g^{-1}, the difference of cation-anion-uptake.

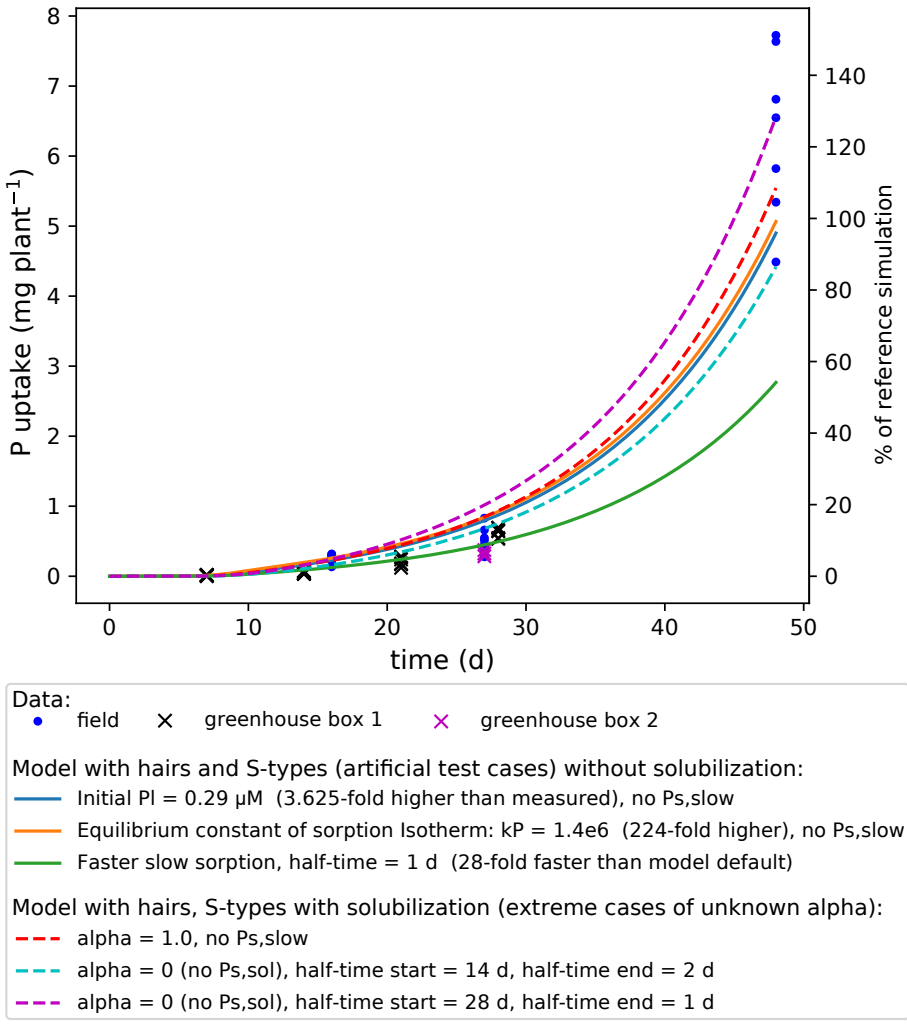

FIGURE S2 Results of simulation runs. Without coupling we would either need a much higher starting P concentration in solution (red line) or a much higher instantaneous solid P phase (violet line). Therefore it is crucial to know the sizes of the pools. None of the simulations were able to match the shape of the exponential curve fit to the data. To reach a higher concentration at the end of the time interval (day 48), the earlier point would be over-estimated even more.

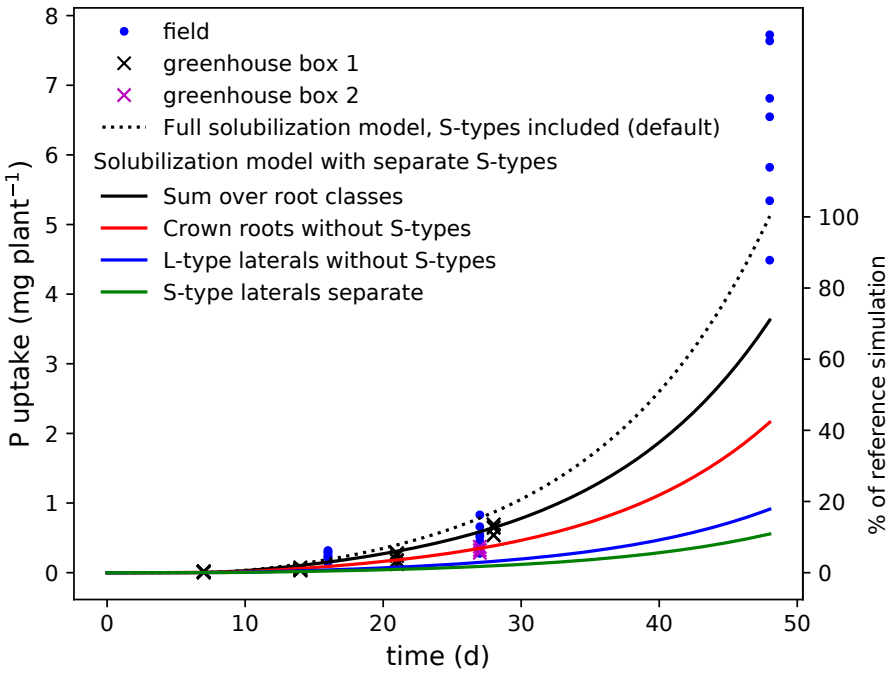

FIGURE S3 Results of S-types simulated separately with the default parameter set, not as part of the crown and L-type rhizosphere. S-type, L-type, and crown root length distribution was (50-33-17%) as in table 2. The ranking of the contribution to uptake reflects the relative surface areas of the root classes. Without placing the S-type laterals in the rhizosphere, most important were thicker roots (crown), then L-type and S-type laterals.

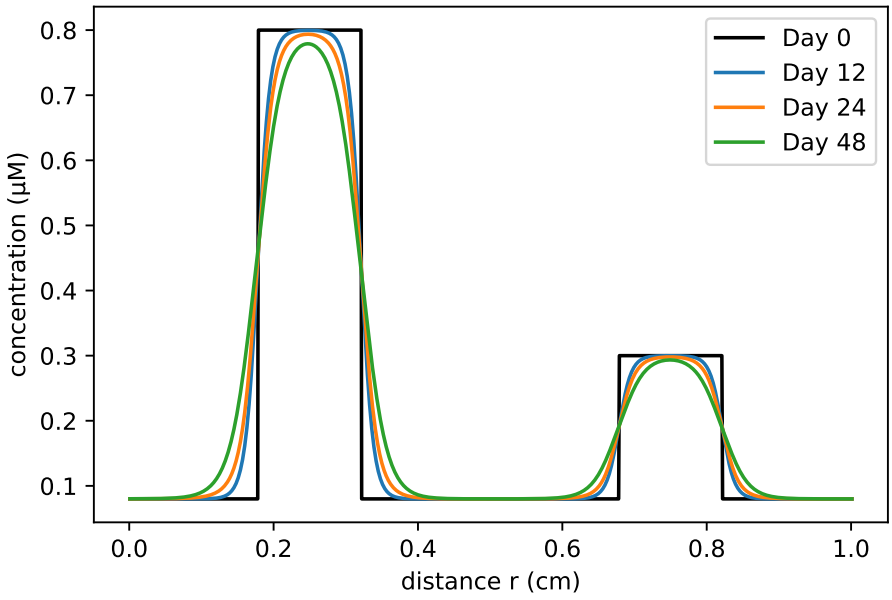

FIGURE S4 Diffusion of P in strongly sorbing soil over 48 days with diffusion coefficient in water of 8.9×10^{-6} cm^2 s^{-1}, impedance factor of 0.24, and soil buffer power of 5440.